Polyamines sustain epithelial regeneration in aged intestines by modulating protein homeostasis

Check for updates

Alberto Minetti[1,13], Omid Omrani [1,13], Christiane Brenner[1,2], Feyza Cansiz[3], Shinya Imada[4], Jonas Rösler[3], Saleh Khawaled[4], Gabriele Allies[3], Sven W. Meckelmann[5], Nadja Gebert[1], Ivonne Heinze[1], Norman Rahnis [1], Jing Lu[1], Katrin Spengler [6], Mahdi Rasa[1,11], Emilio Cirri[1], Regine Heller[6], Ömer Yilmaz [4,7,8], Alpaslan Tasdogan [3,5], Francesco Neri [1,9,10] ✉ & Alessandro Ori [1,12] ✉

Ageing dampens the regenerative potential of intestinal epithelium across species including humans, yet the underlying causes remain elusive. Here we characterized the temporal dynamics of regeneration following injury induced by 5-fluorouracil, a commonly used chemotherapeutic agent, using proteomic and metabolomic profiling of intestinal tissues together with functional assays. The comparison of regeneration dynamics in mice of different ages revealed the emergence of proteostasis stress and increased levels of polyamines following injury exclusively in old epithelia. We show that delayed regeneration is an intrinsic feature of aged epithelial cells that display reduced protein synthesis and the accumulation of ubiquitylated proteins. The inhibition of the polyamine pathway in vivo further delays regeneration in old mice, whereas its activation by dietary intervention or supplementation of polyamines is sufficient to enhance the regenerative capacity of aged intestines. Our findings highlight the promising epithelial targets for interventions aimed at tackling the decline in tissue repair mechanisms associated with ageing.

The ageing process involves a gradual decline of physiological integrity, resulting in diminished organ functionality, reduced regenerative capacities and increased risk of developing pathologies, including cancer[1,2]. A long-standing question in ageing biology and regenerative medicine is defining how tissue repair mechanisms change in the elderly and which strategies can be pursued to ameliorate regeneration without heightening the risk of cancer onset. The small intestine is an excellent model to address these questions given its regenerative capacity mediated by tissue-resident intestinal stem cells. Evidence from different groups has highlighted the contribution of cell-intrinsic alterations, changes in the communication with the stem cell niche and systemic inflammation to the impaired function of old intestinal stem cells[3–5].

However, although ageing is known to delay the regenerative capacity of the small intestine following different types of injury[6,7], little is known about the temporal dynamics of the regeneration process and how these are affected in elderly individuals.

The maintenance of protein homeostasis, also known as proteostasis, is crucial for preserving cellular and tissue function over time, and its dysregulation has been proposed as a hallmark of ageing[8–10]. The mechanisms contributing to proteostasis impairment encompass, among others, alterations in protein turnover rates, a decline in protein degradation and changes in protein quality control mechanisms[1,11–13]. Notably, the requirements for proteostasis maintenance vary across different tissues and cell types[12]. For instance, organs mainly composed

of rarely dividing cells, for example, the brain, are extremely prone to proteostasis impairment and tend to accumulate protein aggregates with age[14,15]. Conversely, in proliferative tissues such as the intestinal epithelium, the evidence for protein homeostasis impairment during ageing is less described, and it mainly arises following stress, for example, upon tissue damage[16,17].

Polyamines are small by-products of food metabolism, and they are gaining relevance in the context of protein homeostasis maintenance and ageing. Polyamines are known to orchestrate important aspects of proteostasis including translation elongation and termination and autophagy[18–21]. Moreover, recent evidence shows polyamines controlling translation rates of hair follicle stem cells, where changes in protein synthesis rates influence stem cell fates[22], highlighting their importance in regulating stem cell adaptation. Spermidine, one of the most active polyamines, enhances translation efficiency via the hypusination of the eukaryotic initiation translation factor 5A (EIF5A)[23]. Hypusinated EIF5A has been shown to both alleviate stalling on motifs containing polyproline tracts and stimulate peptidyl-transfer RNA (tRNA) hydrolysis in translation termination, thus improving translation efficiency[18–21]. Polyamines are also reported to tightly regulate other biological processes, including cellular proliferation, mitochondrial respiration and immune responses[24,25]. Moreover, despite differences among tissues, their abundance seems to decrease with age[26], thus raising attention to their relevance for healthy ageing and cytoprotection.

Strategies aimed to improve intestinal regeneration have been proposed, including dietary interventions based on dietary restriction (DR) and fasting[4,6,7,27–30]. Interestingly, in the context of dietary interventions, recent findings showed that postfast re-feeding (RF) improves intestinal stem cell-mediated regeneration via polyamine metabolism[31]. Whether these pathways contribute to age-related differences in intestinal epithelium regeneration remains elusive.

To model small intestine regeneration, we adopted 5-fluorouracil (5-FU), a widely used chemotherapeutic agent known to inhibit DNA replication and RNA synthesis and affect ribosome function[32–35]. Within the gastrointestinal system, 5-FU induces intestinal mucositis, leading to decreased body weight primarily due to fluid imbalance and food malabsorption. We chose 5-FU because of (1) the mechanism of action targeting both nucleic acids and protein synthesis machinery, (2) the relatively milder effects compared with alternative injury models such as DSS or γ-irradiation and (3) the established age-related differences in intestinal regeneration[6]. Here, investigating the dynamics of intestinal regeneration in young and old mice following a single injection of 5-FU, we found that, upon injury, old intestinal epithelia promote polyamine

metabolism to overcome the emergence of proteostasis stress induced by tissue damage. In addition, we show that the regenerative capacity of old intestines can be restored by activating the polyamine pathway before injury via an intervention based on DR followed by RF.

Results

### Proteome dynamics during intestinal epithelium regeneration

To dissect the temporal dynamics of small intestine regeneration, we collected whole tissue samples from small intestines of male mice on days 2, 5 and 7 after a single injection of 5-FU or vehicle control (phosphate-buffered saline (PBS)) (Fig. 1a). In young mice (3–5 months), 5-FU induced a mild reduction in body weight (~5%) that peaked at 2 days post injection (dpi) and resolved at 5 dpi (Fig. 1b). The effect on body weight was accompanied by histological changes of the intestinal epithelium including a decrease in crypt number (Fig. 1c,d), density of differentiated cells within the villi (Fig. 1c,e), number of phospho-histone H3 (pH3)-positive cells (Fig. 1f) and crypt length (Extended Data Fig. 1a). Although slight variations in temporal dynamics were observed among the different histological parameters, they were all consistent with reduced cell proliferation and tissue renewal at 2 dpi that typically resolved between 5 and 7 dpi.

To monitor the dynamics of intestinal regeneration at the proteome level, we analysed samples from the whole intestinal tissue using label-free data independent acquisition (DIA) mass spectrometry (MS). We quantified 5,627 protein groups with at least two proteotypic peptides across all the timepoints and replicates (Extended Data Fig. 1b). We then used k-means clustering to group proteins that show changes in abundance following 5-FU injection relative to vehicle control (Extended Data Fig. 1c). The majority (>60%) of protein groups quantified showed no change in their abundance. We found 2,204 proteins affected by 5-FU that could be classified into four major clusters according to their abundance profile (Fig. 1g and Supplementary Table 1). The four clusters were enriched for specific pathways (Fig. 1h). These included pathways related to transcription and translation, lipid metabolism, immune response and extracellular matrix organization, among others (Fig. 1i and Extended Data Fig. 1d). Many of these pathways have been functionally linked to intestine regeneration[36–42].

To functionally validate our findings, we focused on cluster 1, which includes multiple components of the minichromosome maintenance (MCM) complex and the ribosome (Fig. 1i and Extended Data Fig. 1e,f). We confirmed reduced protein synthesis on freshly isolated intestinal crypts at 2 dpi using ex vivo puromycin incorporation assay (Fig. 1j,k). In line with reduced protein synthesis, crypts from 2 dpi displayed a drastically reduced organoid-forming capacity that was

Fig. 1 | Identifying proteome dynamics during regeneration of young small intestines. a, A schematic of 5-FU induced regeneration in young mice. i.p., intraperitoneal. **b**, The relative body weight of young mice treated with a single dose of 5-FU or PBS as control. The body weight of each mouse was normalized to its body weight at the time of injection. n = 18 PBS, n = 17 5-FU mice. The red and blue lines indicate the median body weight for each treatment group on each day. The P values were calculated using the two-tailed Welch's t-test by comparing the body weights of 5-FU-treated mice with PBS-treated controls on the indicated day and by two-way ANOVA for overall day and treatment comparisons. **c**, The representative pictures of haematoxylin and eosin (H&E) staining of the small intestine from indicated treatments and timepoints. Scale bars, 50 μm. **d**, The quantification of the number of crypts per millimetre of small intestine in the indicated groups. The PBS-treated mice from different days were combined. Each dot represents one mouse. n = 12 PBS, n = 4 5-FU mice per group. The data are presented as mean ± s.d. The P value was calculated using the two-tailed Welch's t-test. **e**, The quantification of the number of cells per micrometre of villus in the indicated groups. PBS-treated mice from different days were combined. Each dot represents one mouse. n = 11 PBS, n = 4 5-FU mice per group. The data are presented as mean ± s.d. The P value was calculated using the two-tailed Welch's t-test. **f**, Left: the representative pictures of pH3 staining from indicated treatment and timepoint. Scale bar, 100 μm. The asterisks indicate the pH3+

crypts. Right: the percentage of pH3+ crypts in the indicated groups. The PBS-treated mice from different days were combined. Each dot represents one mouse. n = 14 PBS; n = 5 day 2, n = 6 day 5, n = 11 day 7 5-FU. The data are presented as mean ± s.d. The P value was calculated using the two-tailed Welch's t-test. **g**, The classification of protein groups quantified by proteomics according to their abundance changes relative to the PBS controls. **h**, The abundance profiles for the four clusters of proteins affected by 5-FU. The representative REACTOME gene sets significantly enriched in each cluster are shown. Stand., standardized; SLC, solute carrier; ENOS, endothelial nitric oxide synthase. **i**, The abundance profile of ribosome (67 proteins) and MCM (6 proteins) complexes. The protein abundances of individual complex members were normalized to the median complex abundance of PBS-treated mice, and profiles plotted using a locally estimated scatterplot smoothing function. The shaded area around the regression line represents the 95% confidence interval. n = 16 PBS, n = 5 day 2, n = 5 day 5, n = 4 day 7 5-FU. **j**, A scheme of puromycin incorporation assay performed on freshly isolated crypts. **k**, Left: a representative immunoblot for puromycin incorporation. Right: the quantification of puromycin incorporation relative to Ponceau staining (loading control). Each dot represents one mouse. n = 3 mice per group. The data are presented as mean ± s.d. The P value was calculated using the two-tailed Welch's t-test. Panels **a** and **j** created with BioRender.com.
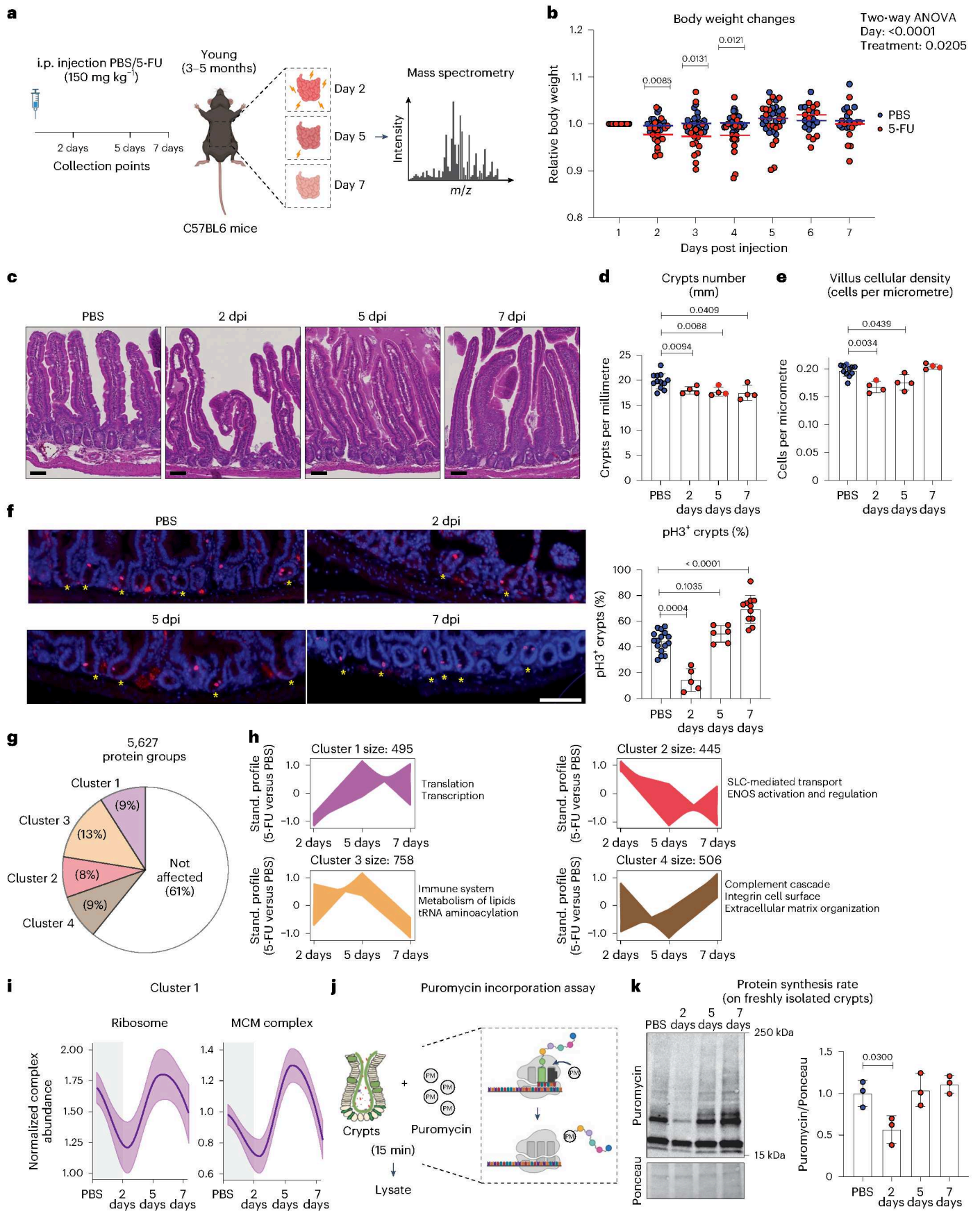
completely restored at 5 dpi (Extended Data Fig. 1g). Together, these data define histological and molecular signatures that characterize different phases of intestinal regeneration and highlight a temporal regulation of the proteome following injury by 5-FU.

Proteostasis stress delays intestinal regeneration in aged intestines

To investigate how ageing affects proteome dynamics during intestinal epithelium regeneration, we performed the same injury experiment using old (22–26 months) mice. Consistent with previous studies[4,6,7,27,28,30], we found that aged mice displayed more pronounced body weight loss (~10% versus 5% in the young) and required 7 days to restore their body weight to a level comparable to the ones of vehicle-treated controls (Fig. 2a and Extended Data Fig. 2a,b). At the histological level, the old epithelia exhibited different dynamics for crypts number (Extended Data Fig. 2c,d), number of pH3-positive cells (Fig. 2b) and density of differentiated cells within the villi (Extended Data Fig. 2c,e) but not crypt length (Extended Data Fig. 2c,f) compared with the young counterparts. To gain insights into the molecular mechanisms of delayed regeneration, we acquired proteomics data from the whole intestinal tissue at the same timepoints post 5-FU injection collected for young animals. For each age group and timepoint, we calculated fold changes relative to vehicle controls and compared protein abundance changes between young and old mice using multivariate analysis of variance (MANOVA) (Fig. 2c). Using k-means clustering, we could identify four major clusters of proteins that displayed different abundance changes in old versus young (446 proteins in total) (Fig. 2d and Supplementary Table 2). The pathway enrichment analysis revealed a network of proteins related to protein homeostasis (hereafter proteostasis) that displayed decreased levels at 2 dpi and increased levels at 7 dpi in old mice compared with young ones (Fig. 2d,e). This cluster included multiple members of the 19S regulatory particle of the proteasome and of the chaperonin-containing TCP-1 complex (CCT), translation initiation factors (EIF1B, EIF2B1 and EIF4A2) and autophagy-related proteins including ATG5 and ATG7 (Fig. 2e,f). Other proteins related to proteostasis also showed significantly different dynamics in the old versus young intestine, although with different profiles (Extended Data Fig. 3a). Interestingly, other proteostasis network components such as ribosomes (Extended Data Fig. 3b) and 20S proteasome (Extended Data Fig. 3c), as well as the MCM complex (Extended Data Fig. 3d), showed identical dynamics in both young and old mice. We confirmed

some of these findings by immunoblot against the autophagy receptor p62 (SQSTM1) and the ribosomal protein RPS6 in an independent set of freshly isolated intestinal crypts (Extended Data Fig. 3e–g). We additionally confirmed that p62 protein level changes were independent of mRNA expression (Extended Data Fig. 3h). In agreement with an impairment of proteostasis, we found increased levels of proteins modified by polyubiquitin chains linked via lysine 48 (K48) at 5 dpi in old mice (Fig. 2g), a marker for protein degradation, but not total ubiquitin (Extended Data Fig. 3i). Conversely, ex vivo measurements of protein synthesis were overall similar in young and old crypts (Fig. 2j), consistent with the similar dynamics of ribosomal proteins (Extended Data Fig. 3b). Together, these data confirm delayed intestinal regeneration in old mice following 5-FU injury. In addition, we identified that delayed regeneration is accompanied by the emergence of a proteostasis stress signature that affects the temporal dynamic of specific proteins in the aged intestinal epithelium and crypts.

Next, we asked whether inducing proteostasis stress is sufficient to delay intestinal regeneration in young mice. We reasoned that interfering with translation elongation during the recovery from 5-FU injury could result in a similar proteostasis impairment as observed in old mice. Thus, we treated young mice with cycloheximide (CHX) or vehicle control at day 3 and 4 post 5-FU or PBS injection (Fig. 2h). The puromycin incorporation assay confirmed a reduction in protein synthesis upon CHX treatment (Extended Data Fig. 4a,b). Consistently, we observed a reduced percentage of pH3+ cells per crypt at day 4 in CHX-treated, 5-FU-injected mice compared with 5-FU-injected control mice (Fig. 2j and Extended Data Fig. 4a). Together with reduced proliferation, CHX treatment led to a more pronounced 5-FU-induced body weight loss at 5 dpi (Fig. 2i). Notably, CHX did not affect body weight in uninjured mice (Extended Data Fig. 4c), underscoring the interaction between 5-FU mediated injury and proteostasis stress in delaying intestinal regeneration. Together, our findings demonstrate that perturbing protein synthesis in young mice is sufficient to disrupt regeneration dynamics following 5-FU, thereby linking proteostasis impairment to delayed regeneration.

Delayed regeneration of old intestinal organoids following 5-FU

Both cell-intrinsic and extrinsic factors influence intestinal regeneration[4,6,7]. To assess to what extent the delayed regeneration of old intestines and the associated proteostasis stress have a cell-intrinsic component, we used intestinal organoids to model the 5-FU injury

---

Fig. 2 | Proteostasis stress delays intestinal regeneration following 5-FU.
a, The relative body weight of young (left) and old (right) mice treated with a single dose of 5-FU or PBS as control. The body weight of each mouse was normalized to its body weight at the time of injection. n = 18 PBS, n = 17 5-FU young mice and n = 12 PBS, n = 14 5-FU old mice. The data are presented as mean ± s.d. The P values were calculated using the two-tailed Welch's t-test by comparing the body weights of 5-FU treated mice with PBS-treated controls on the indicated day. **b**, Left: the representative pictures of pH3 staining from indicated treatments and timepoints. Scale bar, 100 μm. The asterisks indicate the pH3+ crypts. Right: the percentage of pH3+ crypts relative to PBS. At each timepoint, 5-FU values were normalized to the average PBS control mice and expressed as percentage. Each dot represents one mouse. Young mice: n = 5 day 2, n = 6 day 5, n = 11 day 7; old mice: n = 6 day 2, n = 6 day 5, n = 7 day 7. The data are presented as mean ± s.d. The P value was calculated using the two-tailed Welch's t-test for timepoint comparison and two-way ANOVA for overall day and age comparisons. **c**, The workflow for the comparison of protein abundance profiles between young and old mice. PBS-treated young mice: n = 5 day 2, n = 5 day 5, n = 4 day 7. 5-FU-treated young mice: n = 5 day 2, n = 5 day 5, n = 4 day 7. PBS-treated old mice: n = 5 day 2, n = 5 day 5, n = 5 day 7. 5-FU-treated old mice: n = 5 day 2, n = 5 day 5, n = 3 day 7. **d**, The fold change profiles (old versus young, log₂) for the four clusters of proteins that display different dynamics in young and old mice upon 5-FU treatment. Stand., standardized. **e**, The network of proteostasis-related proteins from cluster 1. The protein–protein interactions were derived from STRING[66] using a cut-off of 0.7. **f**, The protein abundance profiles for the components of the

19S proteasome (24 proteins), TriC (7 proteins) complexes, ATG7 and ribosomal proteins (67 proteins). The protein profiles are plotted using a locally estimated scatterplot smoothing function. The shaded area around the regression line represents the 95% confidence interval. n = 14 PBS young, n = 5 day 2, n = 5 day 5, n = 4 day 7 5-FU young; n = 15 PBS old, n = 5 day 2, n = 5 day 5, n = 3 day 7 5-FU old. **g**, Left: a representative immunoblot for the K48-polyubiquitylated proteins. Right: the quantification of K48-polyubiquitylated proteins relatively to Ponceau staining (loading control). Each dot represents one mouse. n = 3 mice per group. The data are presented as mean ± s.d. The P value was calculated using the two-tailed Welch's t-test for timepoint comparison and two-way ANOVA for overall day and age comparisons. **h**, A schematic of the effect of CHX on intestinal regeneration in young mice. **i**, The body weight changes of young mice after 5-FU ± CHX. Each mouse's body weight was normalized to its weight on the day of the PBS or 5-FU injection. At each timepoint, the average body weight change in PBS-treated controls was subtracted from that of 5-FU-treated mice (with or without CHX). This analysis isolates the effect of 5-FU on body weight dynamics between CHX and control groups. The averages were obtained from: n = 3 PBS–PBS, n = 3 PBS–CHX, n = 3 5-FU–PBS, n = 3 5-FU–CHX young mice. The data are presented as mean ± s.d. The P value was calculated using two-way ANOVA for comparisons. **j**, Left: the representative pictures of IHC staining for pH3 at day 4 following 5-FU (±CHX). Scale bars, 100 μm. The arrows indicate the pH3+ cells. Right: the change in number of pH3+ cells per crypt. n = 3 mice per group. The data are presented as mean ± s.d. The P value was calculated using the two-tailed Welch's t-test for group comparison. Panel **h** created with BioRender.com.
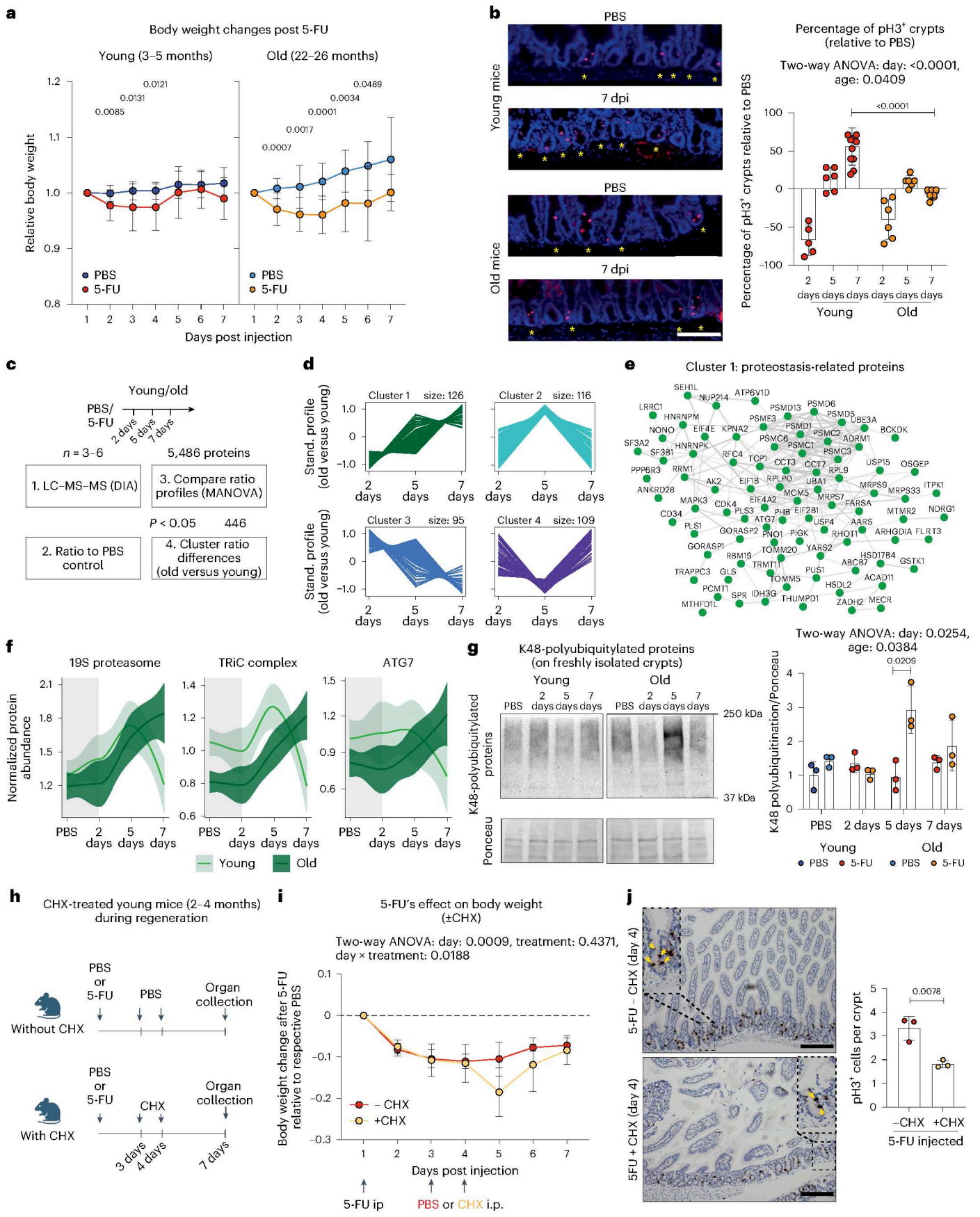
in culture. Small intestinal organoids from young and old mice were treated with different concentrations of 5-FU or vehicle control for 24 h and passaged to wash out 5-FU, and their morphological composition was assessed 3 days later (Fig. 3a). First, we showed that, as expected, 5-FU treatment induced dose-dependent changes in the proportion of cystic, budded or non-regenerating organoids from both young and old mice (Fig. 3b,c). However, old organoids displayed greater sensitivity to 5-FU. At the lowest concentration tested (2.5 and 1.7 μg ml^{-1} of 5-FU), young organoids were able to generate cystic, budded and non-regenerating organoids in a comparable proportion to their PBS control, whereas old organoids showed a significant decrease of budded organoids already at these drug concentrations (Fig. 3b,c). To further define whether intestinal organoids recapitulated other signatures of delayed regeneration observed in vivo, we selected a specific concentration of 5-FU (2.5 μg ml^{-1}), which was the highest concentration displaying age-related morphological differences, and then tested by immunoblot some of the key parameters emerging from in vivo analysis. The intestinal organoids showed proliferation dynamics similar to those observed in vivo: the levels of pH3 were reduced 24 h after 5-FU treatment in both young and old organoids and recovered to baseline 3 days after 5-FU wash out (Fig. 3d). Consistent with reduced proliferation, but differently from freshly isolated crypts (Extended Data Fig. 3j), old organoids displayed reduced protein synthesis levels compared with young, as assessed by puromycin incorporation (Fig. 3e). Next, we performed annexin V assay to quantify the extent of 5-FU induced apoptosis (Extended Data Fig. 4d). No significant changes were detected 24 h after treatment (Fig. 3f). However, 3 days after 5-FU wash out, aged organoids showed a trend towards an increase in apoptosis (Fig. 3f), in line with the morphology analysis (Fig. 3b,c).

Importantly, the delayed regeneration of aged organoids was accompanied by several of the proteostasis stress signatures observed in vivo. The p62/SQSTM1 levels were increased 3 days after 5-FU wash out in old organoids, mirroring in vivo responses (Extended Data Fig. 3e,h). By contrast, K48-polyubiquitylated proteins were elevated at baseline in old organoids but did not show significant differences 3 days after 5-FU wash out (Fig. 3g,h). Together, these data highlight that old intestinal organoids possess reduced regenerative capacity following 5-FU treatment and show some of the signs of proteostasis stress observed in vivo, suggesting an epithelial cell-intrinsic component to the delayed intestinal regeneration.

The polyamine pathway is induced in aged intestinal epithelia following damage

Recent data highlighted that fasting and RF modulate protein synthesis capacity in the intestinal epithelium of young mice due to the mechanistic target of rapamycin complex 1 (mTORC1)-driven regulation of the polyamine pathway[31]. Intrigued by these findings, and given the influence of polyamines on tissue regeneration[24,43–45], we asked whether similar mechanisms might contribute to influencing intestinal regeneration in old mice (Fig. 4a). Thus, we investigated the dynamics of key enzymes involved in polyamine metabolism in our proteome datasets (Fig. 4b). Although individual comparisons between young and old profiles did not reach statistical significance, a consistent trend emerged across multiple enzymes of the pathway. We found ornithine aminotransferase (OAT) to be reduced 2 dpi in both young and old tissues (Extended Data Fig. 5a), concomitantly with reduced ribosomes and protein synthesis. Interestingly, carbamoyl phosphate synthetase 1 (CPS1) and ornithine transcarbamoylase (OTC), the two enzymes involved in the first steps of the urea cycle, were reduced 5 dpi in the old (Extended Data Fig. 5b). Conversely, polyamine oxidase (PAOX), deoxyhypusine synthase (DHPS) and deoxyhypusine hydroxylase (DOHH) showed an increase of abundance at 5 dpi that was more pronounced in the old tissues (Extended Data Fig. 5a). These data suggest an activation of the polyamine metabolism over the urea cycle in aged epithelia following injury, a pattern that closely resembles the observations we made following RF[31]. Therefore, we decided to adopt targeted metabolomics to measure polyamines and related metabolites in freshly isolated crypts following injury. We found comparable levels of polyamines in young and old uninjured crypt samples (Fig. 4c). However, polyamines levels, differently from urea cycle metabolites (Extended Data Fig. 5c,d), varied considerably between young and old following 5-FU injection, with a characteristic increase in abundance at 5 dpi exclusively in aged mice (Fig. 4c). To assess the functional relevance of these findings, we evaluated the total and hypusinated levels of EIF5A, the main downstream effector of the polyamine pathway. The levels of both followed a dynamic consistent with the observed levels of polyamines being increased at 5 dpi in old mice (Fig. 4d). Next, given the known role of hypusinated EIF5A in alleviating ribosome stalling at specific motifs including polyproline tracts[20], we decided to investigate further the dynamics of proteins enriched in these motifs (Fig. 4e). We found several proteins containing these motifs to show distinct dynamics in young and old intestines (Fig. 4f). In particular, proteins containing multiple EIF5A-dependent motifs were over-represented in cluster 2 of our MANOVA analysis (Fig. 4f) (Supplementary Table 2). Among these proteins, we found several proteins known to be required for intestinal regeneration such as the main collagen proteins (COL1A1 and COL3A1) and other extracellular matrix proteins, including fibrillin 1 and 2 (FBN1-2)[46,47] (Fig. 4g). Notably, their expression profile closely resembled the ones of polyamines and downstream effectors (Fig. 4c,d and Extended Data Fig. 5e) of the pathway.

Finally, to test whether the activation of the polyamine pathway is a cell-intrinsic response during regeneration in ageing, we performed

Fig. 3 | Delayed regeneration of organoids from old mice upon 5-FU treatment. a, A scheme of the 5-FU-induced regeneration experiment using intestinal organoids. **b**, The brightfield images of intestinal organoids from the indicated conditions, taken 3 days after PBS or 5-FU wash out. The images are representative of organoid cultures derived from n = 3 young and n = 3 old mice, independently cultured under the different conditions. Scale bars, 200 μm. **c**, The quantification of organoid morphology at day 3 post 5-FU treatment. The bars show the percentage of budded, cystic or non-regenerating organoids from independent organoid cultures derived from young and old mice (n = 3 young and n = 3 old mice). The data are presented as mean ± s.d. The P value was calculated by the two-tailed Welch's t-test comparing the different conditions with young or old PBS control. **d**, Left: a representative immunoblot for the pH3 protein. Right: the quantification of the pH3 level relative to Ponceau staining (loading control). n = 5 mice per group. The data are presented as mean ± s.d. The P value was calculated using the two-tailed Welch's t-test for timepoint comparison and two-way ANOVA for overall day and age comparisons. **e**, Left: a representative immunoblot for the puromycin incorporated proteins. Right: the quantification of the puromycin incorporation relative to Ponceau staining (loading control). n = 4 mice per group. The data are presented as mean ± s.d. The P value was calculated using the two-tailed Welch's t-test for timepoint comparison and two-way ANOVA for overall day and age comparisons. **f**, Left: a representative FACS gating for annexin V assay on old organoids at day 3 after 5-FU wash out. Right: the quantification of the sum of early and late apoptotic cells at the indicated timepoints. n = 6 young; n = 5 old. The data are presented as mean ± s.d. The P value was calculated using the two-tailed Welch's t-test for timepoint comparison and two-way ANOVA for overall day and age comparisons. **g**, Left: a representative immunoblot for the SQSTM1 protein. Right: the quantification of SQSTM1 protein level relative to Ponceau staining (loading control). n = 4 mice per group. The data are presented as mean ± s.d. The P value was calculated using the two-tailed Welch's t-test for timepoint comparison and two-way ANOVA for overall day and age comparisons. **h**, Left: a representative immunoblot for the K48-polyubiquitylated proteins. Right: the quantification of K48-polyubiquitylated protein level relative to Ponceau staining (loading control). n = 5 mice per group. The data are presented as mean ± s.d. The P value was calculated using the two-tailed Welch's t-test for timepoint comparison and two-way ANOVA for overall day and age comparisons. n.s., not significant.
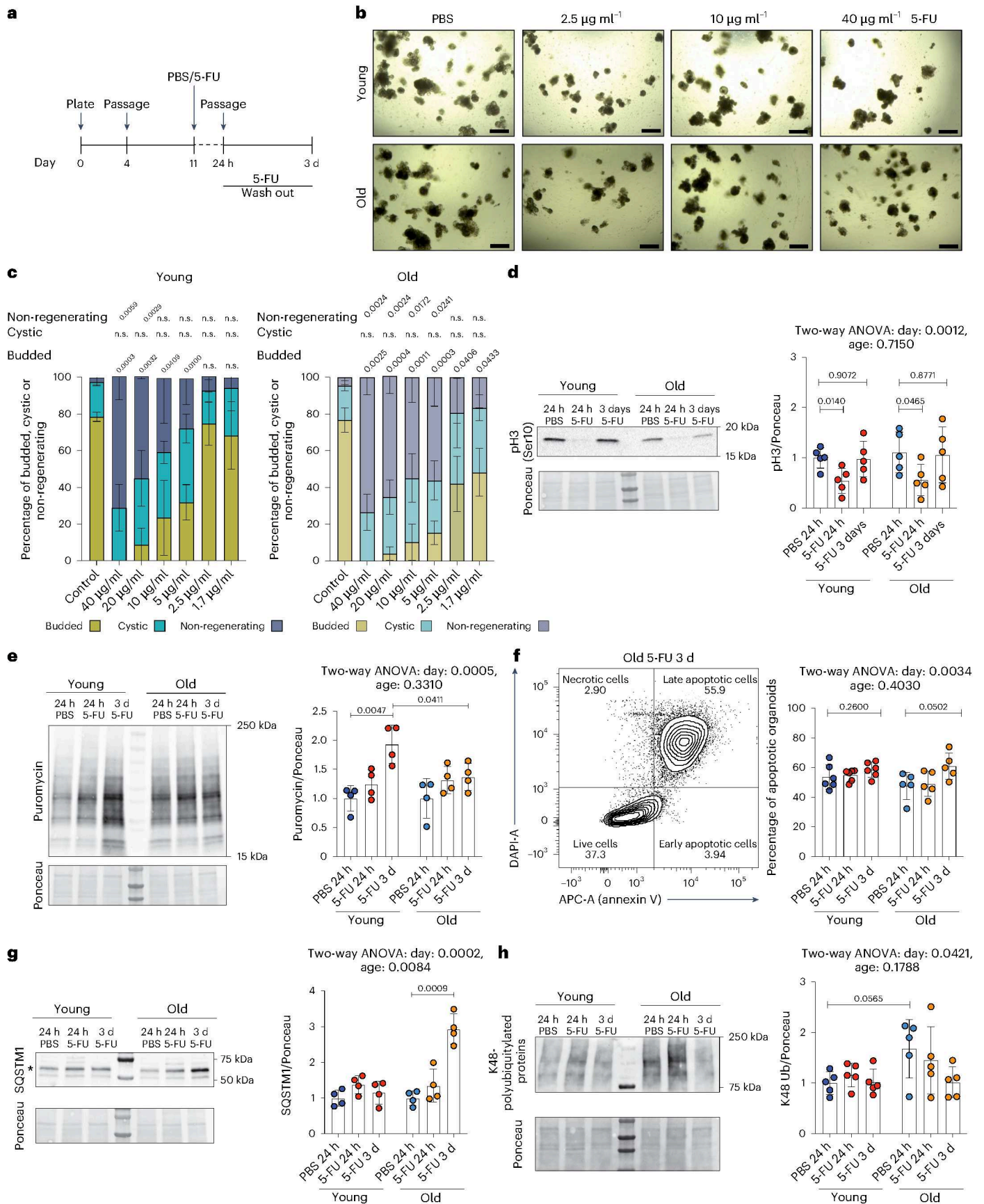
in vitro experiments. When grown in polyamine-free media (Methods), young and old organoids displayed similar morphology (Extended Data Fig. 5f). However, old organoids show reduced hypusinated EIF5A levels with no change in total EIF5A at baseline when compared with their young counterparts (Fig. 4h,i). Interestingly, upon the induction of regeneration by passaging[48,49], old organoids exhibit an approximately twofold increase in hypusinated EIF5A (Fig. 4h,i). The same was not observed in young organoids, which maintained similar levels of hypusinated and total EIF5A (Fig. 4h,i).

Together, these data demonstrate that the polyamine pathway is induced in response to 5-FU in old epithelia likely to sustain proteostasis and the synthesis of key proteins required for intestinal regeneration, such as collagens and other extracellular matrix components. Moreover, the modulation of the polyamine pathway appears to be an intrinsic response that supports regeneration in aged cells, as evidenced by aged intestinal organoids maintaining active polyamine pathway following a regeneration-like stimulus such as mechanical passaging.

Polyamine metabolism is required to sustain small intestinal proteostasis and regeneration

The increased levels of polyamines at 5 dpi, concomitant with the emergence of proteostasis stress, made us hypothesize that the induction of polyamines might be part of an adaptive response of old epithelial cells to injury. To assess the role of the polyamine pathway in intestinal regeneration during ageing, we inhibited ODC1 in old mice using difluoromethylornithine (DFMO)[50,51]. DFMO was administered on days 3 and 4 following the 5-FU treatment to blunt the injury-induced polyamine pathway activation (Fig. 5a). Although DFMO- and vehicle-treated mice exhibited similar body weight changes in the initial days following 5-FU injection, DFMO-treated mice failed to fully recover, showing a significant reduction in body weight on days 10, 11 and 12 post treatment compared with controls (Fig. 5b). The proliferation was also reduced, as indicated by a lower percentage of pH3+ cells per crypt at day 12 post 5-FU (Fig. 5c), highlighting the role of polyamines in supporting cell proliferation and regeneration in old intestines.

Next, we asked whether polyamine pathway perturbation is sufficient to affect regeneration also in young animals. To this end, we used Odc1[loxp/loxp]:Villin-CreERT2 mice, in which Odc1 is selectively ablated in epithelial cells upon tamoxifen (TAM) administration. We injected 5-FU in young Odc1^{fl/fl}:Villin-CreERT2 mice and littermate controls and followed their body weight for 7 days. We found that the knockout (KO) of Odc1 alters the body weight profiles in 5-FU injected mice (Fig. 5d) but not in control, PBS-injected mice (Extended Data Fig. 6a). A histological analysis of intestinal tissues at day 7 following 5-FU revealed a modest but significant effect of ODC1 deficiency on villi cellular density but no effect on crypt number (Fig. 5e–g and Extended Data Fig. 6b–d). Further, the proteome analysis revealed a positive

correlation between the protein changes induced by 5-FU in control mice (5-FU versus PBS injection) and the effect of ODC1 KO (ODC1 KO versus wild-type (WT) mice both groups injected with 5-FU) (Fig. 5h and Supplementary Table 3). The latter analysis indicates that the effect of 5-FU on the proteome of intestinal cells is exacerbated, or the recovery is delayed, in ODC1 KO mice. In addition, we queried the MS data for changes in proteostasis-related proteins induced by ODC1 KO. In ODC1 KO samples, we found modest but significant alterations in multiple proteostasis components including increased levels of proteasome (PSMD1, PSMA5 and PSMB7) and TRiC complex (CCT8) subunits (Fig. 5i) that were also detected in old animals post 5-FU injection (Fig. 2f and Supplementary Table 3).

Together, these data demonstrate that polyamine pathway deficiency, whether through pharmacological inhibition in ageing or genetic KO of Odc1 in young mice, is sufficient to influence the body weight recovery and regeneration dynamics following 5-FU. Furthermore, the proteomic analysis of ODC1 KO samples supports a mechanistic link between the polyamine pathway, proteostasis and intestinal regeneration.

Impact of RF on the regenerative capacity of old intestines

Having demonstrated that the inhibition of the polyamine pathway is sufficient to delay intestinal regeneration, we asked whether interventions known to elevate polyamine levels can restore the regenerative capacity of the old intestine to a youthful state. We have previously shown that increased levels of polyamines following postfasting RF enhance the regenerative capacities of intestinal stem cells[31] and that DR followed by RF can reverse ageing proteome signatures in intestinal crypts[30] affecting multiple proteostasis components including EIF5A (Fig. 6a and Extended Data Fig. 7a). Therefore, we tested whether such a dietary intervention (DR + RF) would be sufficient to restore regenerative capacity upon 5-FU in old mice. First, we confirmed that RF following 1 month of 30% DR increased the levels of both total and hypusinated EIF5A in intestinal crypts (Extended Data Fig. 7b). The total and hypusinated EIF5A peaked 2 days after the beginning of RF and declined thereafter, reaching the levels of ad libitum (AL)-fed mice after 9 days (Fig. 6b and Extended Data Fig. 7b). Importantly, the levels of hypusinated EIF5A correlated with the concentration of polyamines in intestinal crypts, indicating pathway activation induced by RF (Fig. 6c). Based on these data, we subjected both young and old mice to 1 month of DR followed by 2 days of RF before 5-FU injection (Fig. 6d). Mice fed AL or that underwent DR without RF served as control groups. The dietary interventions had the expected effect on the mice's body weight before 5-FU injection (Extended Data Fig. 7c). When analysing body weight curves, we noted that both DR and DR + RF prevented body weight loss following 5-FU injection in young mice. However, in old mice, only DR + RF was sufficient to prevent body weight loss (Fig. 6e,f). Next,

Fig. 4 | Polyamine pathway elevation upon 5-FU in the aged intestinal epithelium. a, A schematic representation of the dynamics of protein synthesis comparing our damage–regeneration model with the fasting–RF model from Imada et al. 2024. **b**, A schematic representation of the polyamine biosynthesis and ornithine metabolism pathways. **c**, The LC–MS quantification of polyamines from crypts lysate. Each dot represents one mouse. $n = 4$ mice per condition. The data are presented as mean ± s.d. The P value was calculated using the two-tailed Welch's t-test for timepoint comparison and two-way ANOVA for overall day and age comparisons. **d**, Left: a representative immunoblot for hypusinated EIF5A and total EIF5A proteins. Right: the quantification of hypusinated EIF5A and total EIF5A relative to Ponceau staining (loading control). Each dot represents one mouse (young: $n = 3$; old: $n = 5$ per each indicated condition). The data are presented as mean ± s.d. The P value was calculated using the two-tailed Welch's t-test for timepoint comparison and two-way ANOVA for overall day and age comparisons. **e**, The top 29 motifs that depend on hypusinated EIF5A for efficient translation according to ref. 20. Pro–Pro, proline–proline. **f**, The distribution of proteins enriched in hypusinated EIF5A-dependent motifs across clusters that show distinct dynamics in young and old mice (see Fig. 2c for cluster assignment

and Fig. 2d for cluster profiles). The cluster numbers and their corresponding protein amounts (in brackets) are displayed on the x axis. Highlighted are the proteins that contain the highest number of hypusinated EIF5A-dependent motifs. The black line of each boxplot represents the median value, and the whiskers extend to 1.5× the interquartile range. The P value was calculated using Wilcoxon rank sum. **g**, The protein abundance profiles of the COL1A1, COL15A1 and FBN2 proteins. The protein profiles are plotted using a locally estimated scatterplot smoothing function. The shaded area around the regression line represents the 95% confidence interval. $n = 14$ PBS young, $n = 5$ day 2, $n = 5$ day 5, $n = 4$ day 7 5-FU young; $n = 15$ PBS old, $n = 5$ day 2, $n = 5$ day 5, $n = 3$ day 7 5-FU old. **h**, A schematic of young and old organoids in polyamine-free basal media. On day 12, young and old organoids were passaged to induce regeneration. The polyamine pathway activation was assessed both at baseline (on fully developed organoids, before passaging) and 3 days later. **i**, Left: a representative immunoblot for hypusinated EIF5A and total EIF5A proteins. Right: the quantification of hypusinated EIF5A and total EIF5A normalized to Ponceau staining. $n = 4$ mice per group. The data are presented as mean ± s.d. The P value was calculated using the two-tailed Welch's t-test for comparisons.
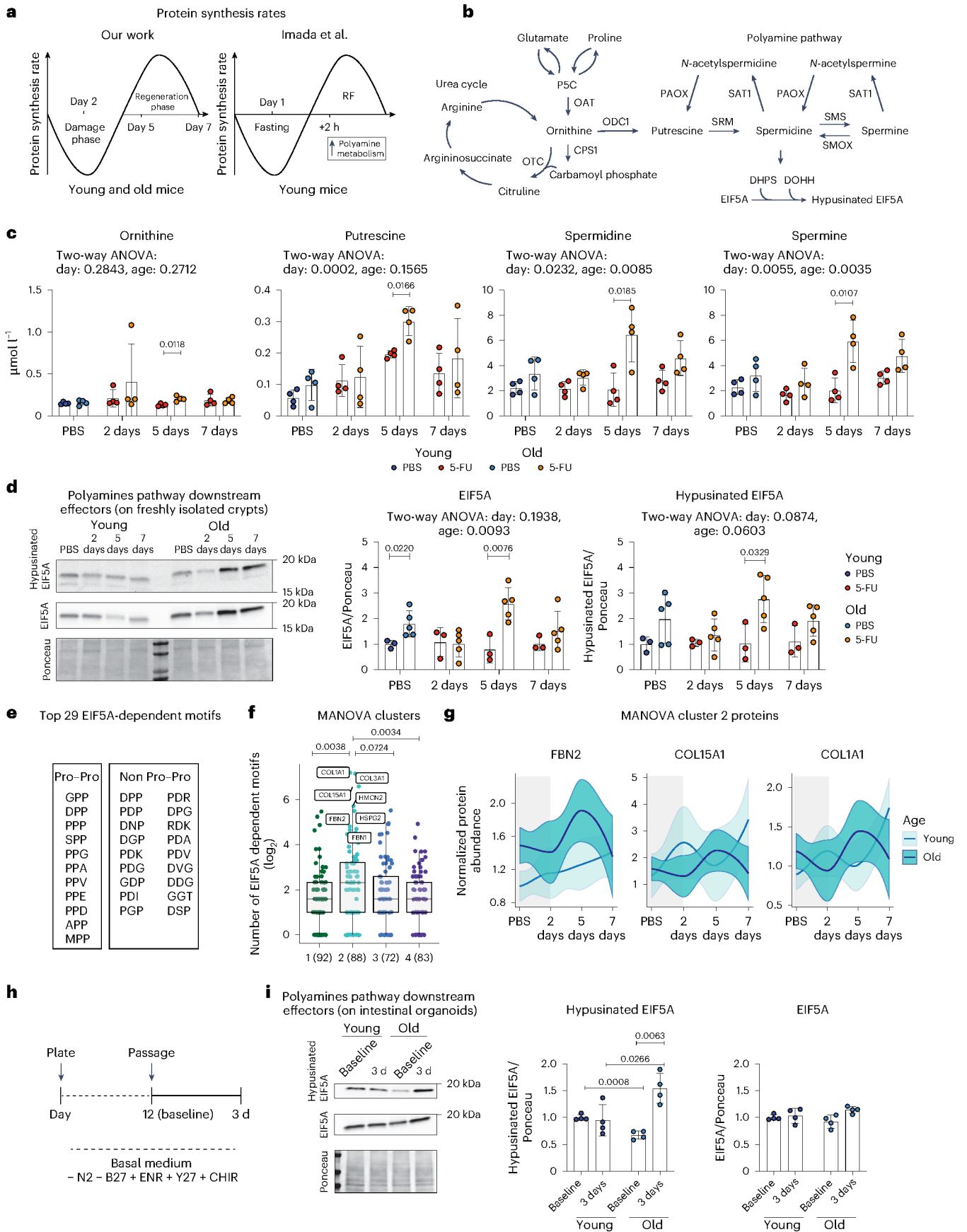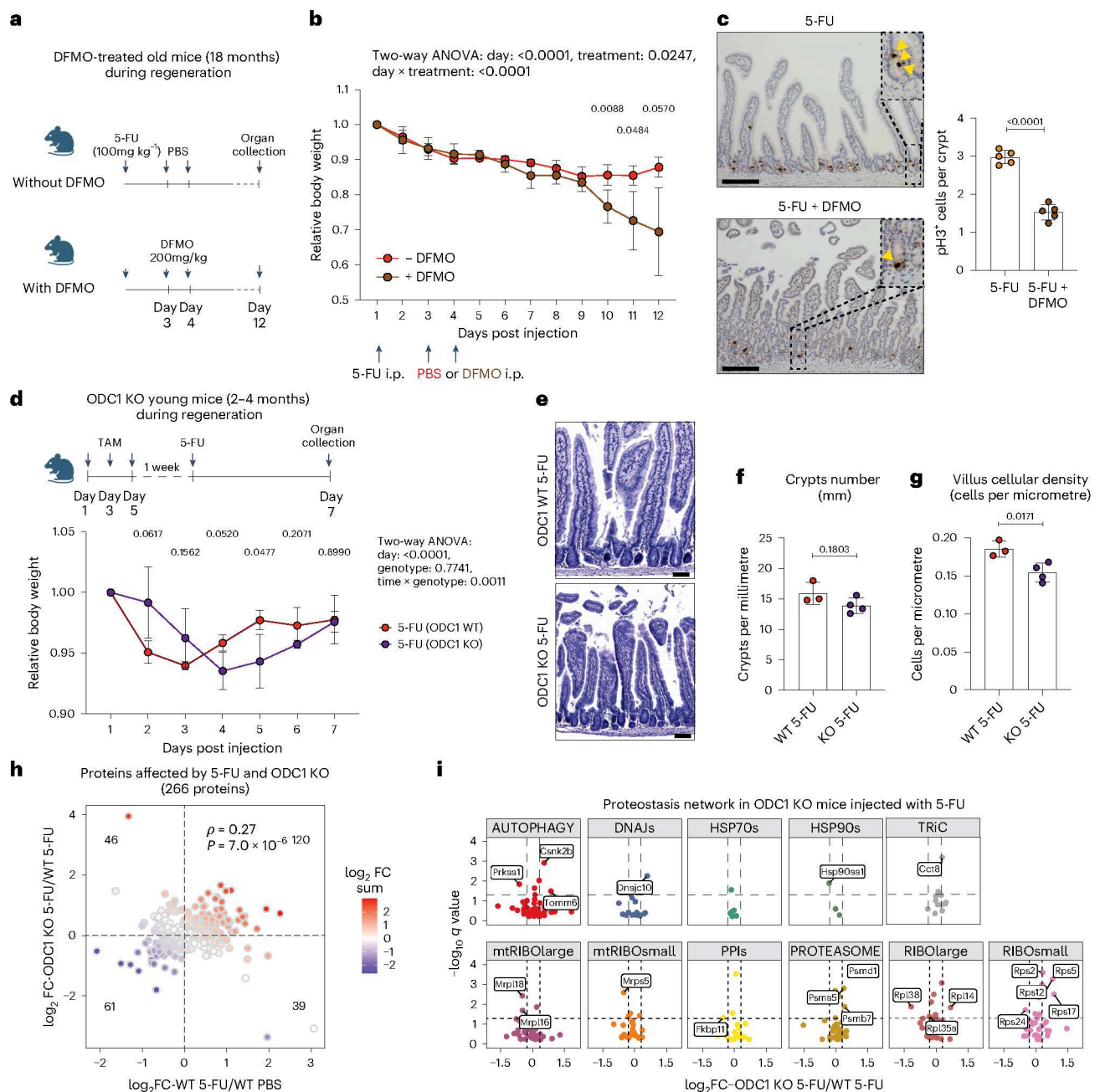
Fig. 5 | Polyamine pathway deficiency impairs intestinal regeneration in young and old mice. a, A schematic of 5-FU treatments in old mice with and without DFMO. **b**, The relative body weight of old mice treated twice with DFMO or vehicle control after a single dose of 5-FU (100 mg kg⁻¹). The body weight of each mouse was normalized to its body weight at the day of injection. $n = 5$ 5-FU + DFMO, $n = 5$ 5-FU − DFMO mice. The data are presented as mean ± s.d. The P value was calculated using the two-tailed Welch's t-test for timepoint comparison and two-way ANOVA for overall comparisons. **c**, Left: the representative pictures of IHC staining for pH3 at day 12 following 5-FU (±DFMO). Scale bars, 100 μm. The arrows indicate the pH3⁺ cells. Right: the change in the number of pH3⁺ cells per crypt; $n = 5$ mice per group. The data are presented as mean ± s.d. The P value was calculated using the two-tailed Welch's t-test for group comparison. **d**, Top: a schematic of ODC1 KO induction and 5-FU treatment. Bottom: the relative body weight of young ODC1 KO and WT mice treated with a single dose of 5-FU. The body weight of each mouse was normalized to its body weight at the day of injection. $n = 4$ ODC1 KO, $n = 3$ ODC1 WT mice. The data are presented as mean ± s.d. The P value was calculated using the two-tailed Welch's t-test for timepoint comparison and two-way ANOVA for overall day, treatment and day x treatment comparisons. **e**, The representative H&E stainings of ODC1 KO and WT small intestines at 7 days post 5-FU injection. Scale bars, 50 μm. **f**, The quantification of the number of crypts per millimetre of small

intestine in the indicated groups (7 dpi). Each dot represents one mouse. $n = 3$ 5-FU ODC1 WT group; $n = 4$ 5-FU ODC1 KO group. The data are presented as mean ± s.d. The P value was calculated by the two-tailed Welch's t-test. **g**, The quantification of the number of cells per micrometre of villus in the indicated groups (7 dpi). Each dot represents one mouse. $n = 3$ 5-FU ODC1 WT group; $n = 4$ 5-FU ODC1 KO group. The data are presented as mean ± s.d. The P value was calculated by the two-tailed Welch's t-test. **h**, A comparison of protein fold changes (FC) induced by 5-FU in ODC1 WT mice (x axis) and the effect of ODC1 KO on 5-FU injected mice (y axis). The proteomics data are from intestinal crypts collected at 7 dpi. The proteins significant ($q < 0.05$) in both comparisons are plotted. The colour code indicates the sum of the log₂FC from the two comparisons. The number of proteins in each quadrant is indicated. The correlation between the two treatments was assessed using Spearman's correlation test. $n = 3$ PBS, $n = 3$ 5-FU mice ODC1 WT group; $n = 4$ 5-FU mice ODC1 KO group. The q values are from Spectronaut differential abundance analysis. **i**, The effect of ODC1 KO on proteostasis-related proteins. The volcano plots are based on the comparison of ODC1 KO versus WT in 5-FU injected mice. The significantly affected (absolute log₂FC >0.3 and $q < 0.05$) proteins are shown. $n = 3$ 5-FU mice ODC1 WT group; $n = 4$ 5-FU mice ODC1 KO group. The q values are from Spectronaut differential abundance analysis. Panels **a** and **d** created with BioRender.com.
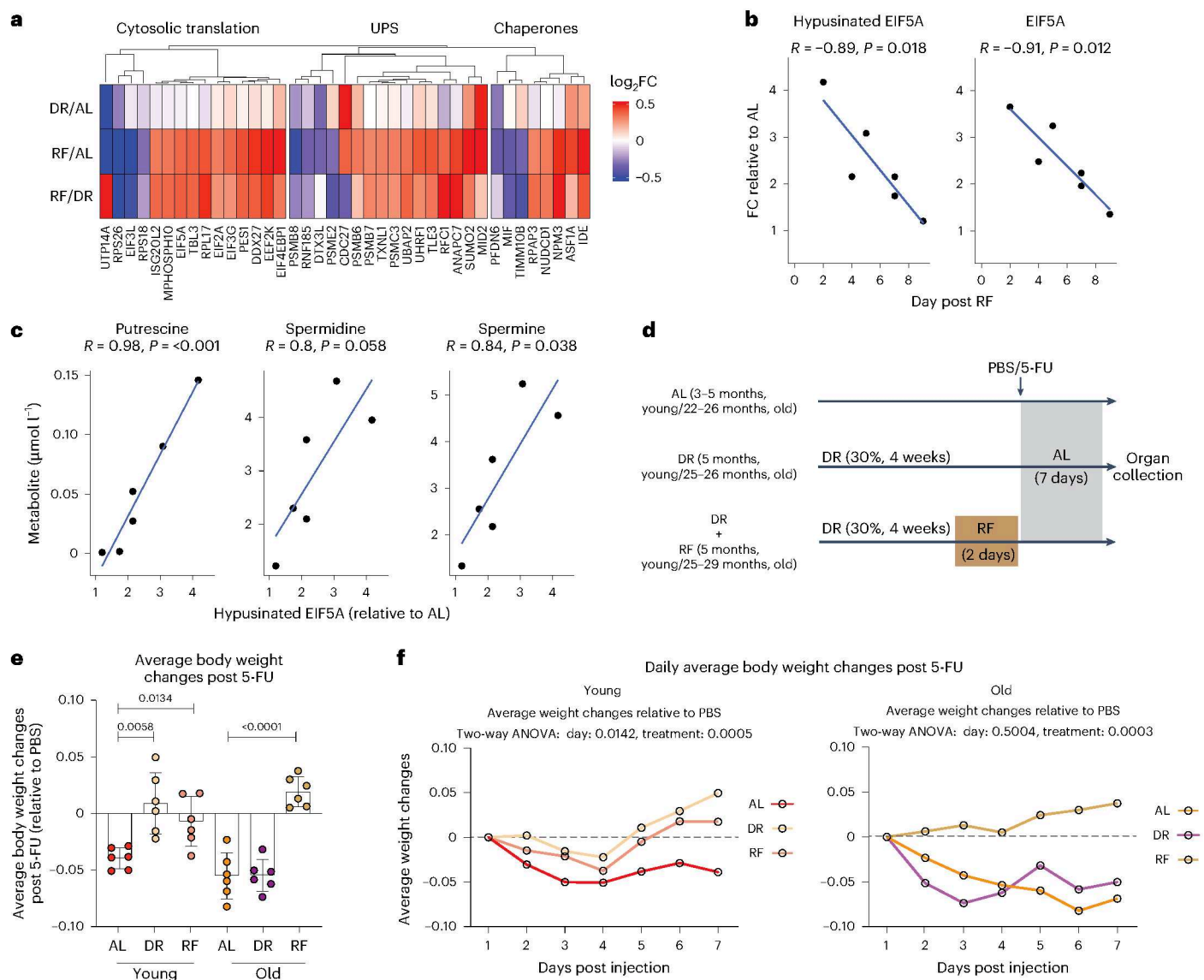
Fig. 6 | Effect of DR followed by RF on intestinal epithelium regeneration.
a, A heat map of fold changes (log$_2$FC) for significantly affected proteins (absolute log$_2$FC >0.3 and q < 0.05) related to proteostasis from aged mice after DR or DR + RF treatments. UPS, ubiquitin proteasome system. n = 4 mice per group. **b**, The levels of total and hypusinated EIF5A from aged mice at different days after RF, quantified by immunoblot (Extended Data Fig. 6b). **c**, The correlation between hypusinated EIF5A and polyamines levels measured on the same intestinal crypt samples from aged mice that underwent DR followed by different days of RF. The R values represent Pearson correlation coefficient, and the P values are the result of the association test between the variables based on Pearson's product moment correlation coefficient. **d**, The scheme of AL, DR and DR + RF treatments prior PBS or 5-FU injection. **e**, The relative average body

weight changes after 5-FU. The body weight of each mouse was normalized to its body weight at the time of injection. For each timepoint, the average body weight of the vehicle treated group was subtracted from the average body weight of the 5-FU one. Each dot represents the daily average body weight change after 5-FU, n = 6. The averages were obtained from n = 16 PBS, n = 15 5-FU AL, n = 4 PBS, n = 6 5-FU DR, n = 5 PBS, n = 7 5-FU RF young mice and n = 17 PBS, n = 15 5-FU AL, n = 10 PBS, n = 16 5-FU DR, n = 7 PBS, n = 17 5-FU RF old mice. The P value was calculated by the two-tailed Welch's t-test. **f**, The daily relative body weight changes induced by 5-FU in young (left) and old (right) mice. The body weights were calculated as in **e**. The P value was calculated using two-way ANOVA for overall day and treatment comparisons. The data in **a** are from ref. 30.

we examined the effects of dietary interventions on polyamines and downstream effectors in old mice after injury. The DR + RF mice showed a trend towards increased total and hypusinated EIF5A already at 2 dpi (Extended Data Fig. 7d). Similarly, protein synthesis assessed by ex vivo puromycin incorporation, appeared elevated at 2 dpi in DR + RF mice but only at 5 dpi in AL and DR groups (Extended Data Fig. 7e). A similar trend was observed for pH3, suggesting anticipated and enhanced proliferation in DR + RF, injured mice (Extended Data Fig. 7f).

Together, these data highlight that a dietary intervention based on DR followed by 2 days of RF increases both polyamines levels and downstream effectors in aged mice. Importantly, it also mitigates body

weight loss after 5-FU injury, enhances protein synthesis and increases proliferation, thereby suggesting accelerated recovery.

Polyamine supplementation before injury enhances intestinal regeneration in old mice

As RF promotes regeneration through multiple pathways[52,53], we asked whether polyamine supplementation is sufficient to improve intestinal regeneration in old mice. Thus, we supplemented old mice with equimolar amounts of spermidine and spermine via oral gavage and confirmed an approximately twofold increase in their levels by targeted metabolomics on freshly isolated intestinal crypts (Fig. 7a).
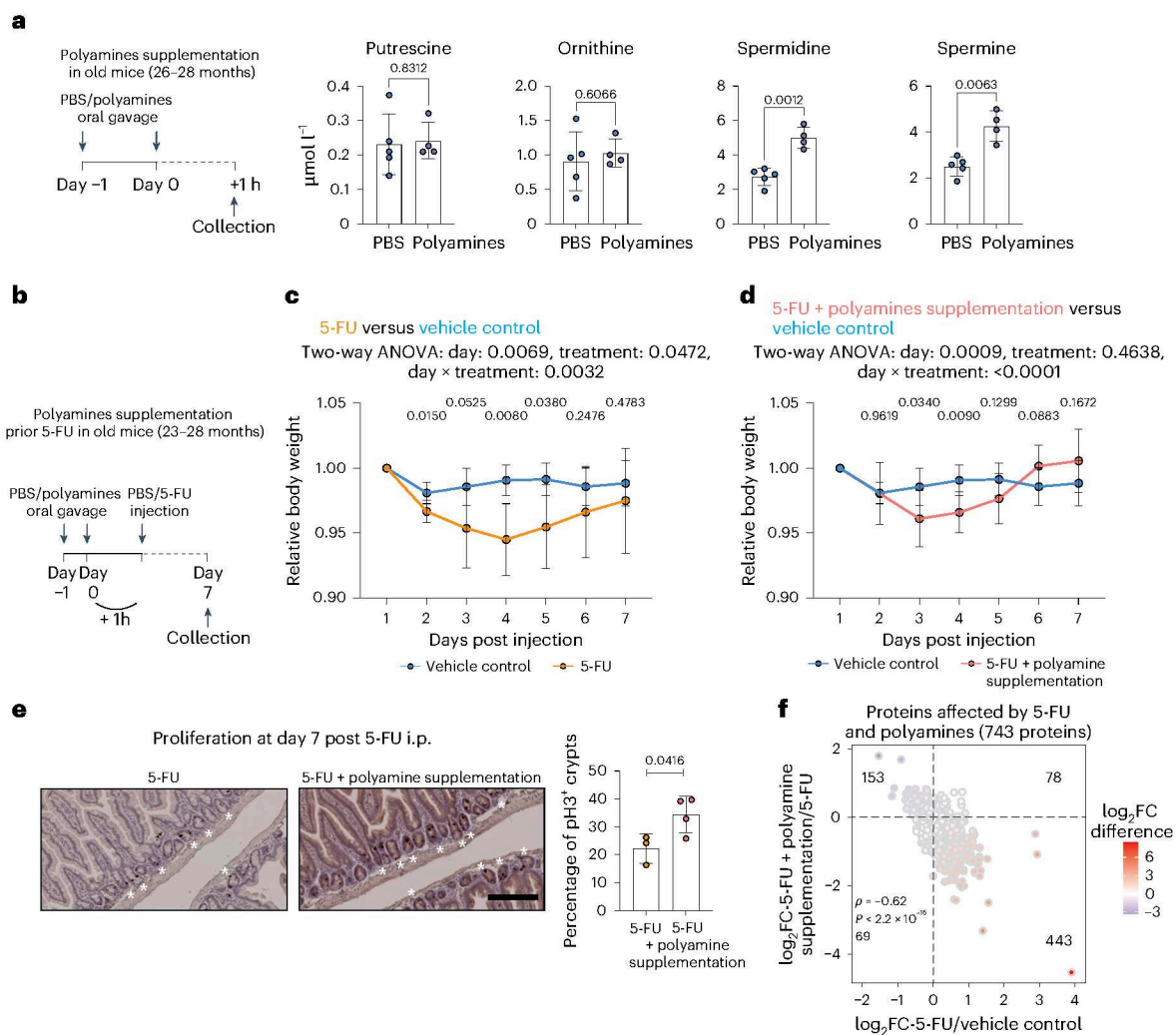
Fig. 7 | Effect of polyamine supplementation on intestinal epithelium regeneration in old mice. a, Left: a schematic of polyamines supplementation in old mice. Right: the LC–MS quantification of polyamines from crypts lysate. Each dot represents one mouse. $n = 4$ (polyamines gavage) $n = 5$ (PBS gavage) mice per condition. The data are presented as mean ± s.d. The P value was calculated using the two-tailed Welch's t-test for group comparison. **b**, A schematic of polyamines supplementation before 5-FU injury in old mice. **c**, The relative body weight of old mice orally gavaged with PBS prior 5-FU (5-FU) or PBS (vehicle control) injection. The body weight of each mouse was normalized to its body weight at the time of injection. $n = 6$ for vehicle control group, $n = 6$ for 5-FU group. The data are presented as mean ± s.d. The P value was calculated using the two-tailed Welch's t-test for timepoint comparison and two-way ANOVA for overall comparisons. **d**, The relative body weight of old mice orally gavaged with polyamines prior 5-FU injection (5-FU + polyamines supplementation) or PBS prior PBS injection (vehicle control). The body weight of each mouse was normalized to its body weight at the time of injection. The data are presented as mean ± s.d. $n = 6$ for vehicle control group, $n = 7$ for 5-FU + polyamines supplementation group. The

P value was calculated using the two-tailed Welch's t-test for timepoint comparison and two-way ANOVA for overall comparisons. **e**, Left: the representative pictures of IHC staining for pH3 at day 7 following 5-FU (± polyamines gavage). Scale bar, 200 μm. The asterisks indicate the pH3+ crypts. Right: the change in % of pH3+ crypt; $n = 3$ mice 5-FU group; $n = 4$ mice 5-FU + polyamines group. The data are presented as mean ± s.d. The P value was calculated using the two-tailed Welch's t-test for group comparison. **f**, A comparison of protein fold changes (FC) induced by 5-FU in old mice (x axis) and the effect of polyamines supplementation on old, 5-FU injected mice (y axis); proteomics data from intestinal crypts collected at 7 dpi. The proteins plotted in both comparisons were filtered for significance on the basis of q values ($q < 0.05$) calculated by Spectronaut using the unpaired t-test between replicates followed by correction for multiple testing. The colour code indicates the difference of the $\log_2$FC between 5-FU and polyamines supplementation effects. The number of proteins in each quadrant is indicated. The correlation between the two treatments was assessed using Spearman's correlation test. $n = 6$ vehicle control, $n = 6$ 5-FU; $n = 7$ 5-FU + polyamines supplementation.

We assessed regeneration dynamics following 5-FU-mediated injury by analysing body weight, histology and proteomic analysis of intestinal tissues at 7 dpi. We found that polyamine supplementation reduces the loss of body weight and accelerates its recovery compared with vehicle control (Fig. 7b–d). The body weight data were supported by pH3 stainings indicating a higher number of proliferating cells at 7 dpi in polyamine-supplemented mice (Fig. 7e). Consistently, the proteome analysis revealed a negative correlation between the protein changes induced by 5-FU in control mice (5-FU versus vehicle control) and the effect of polyamines (polyamines supplemented versus control mice

both groups injected with 5-FU) (Fig. 7f and Supplementary Table 4). The latter analysis indicates that the effect of 5-FU on the proteome of intestinal cells is reduced, or the recovery is accelerated, in polyamines supplemented mice. Notably, we observed that polyamines had a positive effect on mouse body weight and percentage of pH3+ crypts also in uninjured mice (Extended Data Fig. 8a–c), suggesting that the beneficial effect of polyamine supplementation might extend beyond 5-FU based injury. Together, these data demonstrate that polyamine supplementation is sufficient to improve regeneration post 5-FU injury in old mice.

Discussion

Multiple studies have indicated that old mice show a delay in the regeneration of intestinal tissue upon different types of injury compared with young mice[6,7]. Here, using proteomics, we temporally dissected the phases of intestinal epithelium regeneration and compared protein dynamics in young versus old mice, uncovering proteomic and metabolomic changes upon damage and regeneration. The intestinal tissue from young mice showed a strong reduction in proliferation 2 days following 5-FU injection, accompanied by a decrease in proteins related to transcription and translation. Whereas the body weight of young mice recovered at day 5 post injury, old mice required 2 days longer despite showing similar protein synthesis and translation machinery dynamics. The delayed regeneration of old mice was accompanied by the emergence of multiple signs of proteostasis stress exemplified by the accumulation of K48-polyubiquitylated proteins at day 5 post injury. Notably, we demonstrated that pharmacologically interfering with translation elongation using CHX is sufficient to disrupt regeneration dynamics in young mice, thereby linking proteostasis impairment to delayed regeneration.

We established a 5-FU-induced regeneration model in organoid cultures to address the extent to which the delayed regeneration of the old intestine is a cell-intrinsic feature of epithelial cells. We uncovered that intestinal organoids, once challenged with 5-FU, pass through similar regeneration phases as observed in vivo, encompassing changes in protein synthesis and proliferative capacity. Moreover, organoids from old mice showed delayed regeneration compared with young ones and recapitulated some of the proteostasis stress signatures observed in vivo, for example, p62/SQSTM1 accumulation. These data indicate that cell-intrinsic differences in proteostasis might contribute to the delayed regeneration of old intestines in addition to changes in niche-derived[6,7,54] and systemic factors[4,5].

Concomitantly to the emergence of proteostasis stress signatures, we observed that old intestines activate pathways that are typically linked to improved protein homeostasis, such as chaperones and polyamines. Although the causes of proteostasis defects induced by regeneration in old mice remains unclear, we speculate that the activation of these pathways is part of an adaptive response mounted by old intestinal cells to overcome the stress induced by the increase of protein synthesis during regeneration (Extended Data Fig. 8d). In line with this hypothesis, we found that proteins containing specific motifs known to depend on hypusinated EIF5A for efficient translation[20] cluster together following damage, and their abundance profiles follow precisely the dynamics of polyamine pathway activation. Most of these proteins relate to the extracellular matrix, including fibrillin 1 and 2 (FBN1 and FBN2) and main collagen proteins such as COL1A1 and COL3A1, whose implication in intestinal tissue repair has been previously documented[46,47]. In addition, we have shown that the inhibition of protein synthesis in vivo by CHX is sufficient to delay regeneration also in young mice. Together, these independent lines of evidence point to defects in protein synthesis as the most likely source of proteostasis defects induced by injury in old intestinal epithelia.

A decline in polyamines has been associated with ageing in different tissues, and their supplementation has been shown to be sufficient to increase the median life span of flies, worms and mice[19,55,56]. However, our data indicate that polyamines in mouse small intestines do not decline with age, suggesting that they might not contribute to age-related tissue dysfunction under homeostatic or uninjured conditions. Nonetheless, following tissue damage, their functions became relevant, suggesting that they act as stress response metabolites regulated during and/or after injury. Consistent with this observation, gut ischaemia–reperfusion injury in aged individuals has been shown to increase *Odc1* levels alongside activation of unfolded protein response pathway[16]. These data further support the correlation between damage, proteostasis stress and induction of polyamines in aged gut epithelia in humans.

Emerging evidence shows that polyamines can originate from microbiota or immune cells and then be uptaken by epithelial cells and exert their functions to improve both tissue homeostasis and regeneration[24,57,58]. Indeed, their supplementation in vivo has been shown to promote young mouse colonic epithelium regeneration through increased epithelial proliferation and M1/M2 macrophage rebalancing[24]. Similarly, polyamine pathway blockage via *Dhps* deletion has been shown to worsen dextran sulfate sodium-induced colitis in young mice[44,45]. Here, we show that the conditional KO of ODC1 in epithelial cells mildly affects regeneration in young mice and leads to significant changes in several proteostasis components, highlighting how defects in polyamine metabolism are associated with disrupted protein homeostasis during epithelial regeneration. Extending these findings to the ageing context, we found that the pharmacological inhibition of ODC1 in aged mice significantly impaired body weight recovery and disrupted cell proliferation following 5-FU-induced injury.

Although polyamines are generally considered safe and potentially beneficial for tissue regeneration, recent evidence has raised concerns about their possible role in promoting tumour development. On the one hand, polyamine supplementation has been shown to play protective roles in both colitis-associated and sporadic carcinogenesis models by supporting the gut microbiota and reducing colon inflammation[44,45]. On the other hand, once tumours are established, they are known to depend on polyamines, as the inhibition of key enzymes involved in their synthesis has been shown to suppress tumour growth[59–61]. Considering the multistep nature of cancer development, these findings suggest that polyamines may have different effects depending on tumour stage (onset versus progression) and type.

In line with these observations, it has been recently reported that polyamines are induced during the RF phase after fasting. In that context, they have been shown to both enhance protein synthesis rates and intestinal stemness while also increasing tumour initiation upon *Apc* deletion[31]. Collectively, this evidence supports a role for polyamines in stem cell maintenance and tissue repair, while also highlighting the potentially harmful effects in tumour onset.

Dietary interventions involving caloric restriction followed by RF have been shown to enhance tissue homeostasis and regeneration across multiple organs[62–65]. Accordingly, our data show that 1 month of DR followed by 2 days of RF activates the polyamine pathway and prevents 5-FU induced body weight loss in aged mice, while also enhancing protein synthesis and cellular proliferation.

Importantly, although RF may exert its beneficial effects through multiple pathways[52,53], we found that direct polyamine supplementation in aged mice was sufficient to improve body weight recovery, enhance proliferation and restore proteomic changes induced by 5-FU, suggesting that polyamines substantially contribute to the beneficial effects observed with DR and RF. Moreover, the effects of polyamine supplementation may extend beyond 5-FU induced injury, as uninjured mice treated with polyamines exhibited an increase in body weight and enhanced intestinal epithelial proliferation.

Altogether, our results suggest that the activation of the polyamine pathway is one of the underlying mechanisms mediating the beneficial effect of post-DR RF in old mice. Ultimately, given that 5-FU is elective therapy for multiple types of cancer, and from the perspective of regenerative medicine, our study provides evidence that the modulation of polyamine pathway activation via dietary interventions or direct oral supplementation might represent a valid strategy to promote tissue recovery and alleviate the gastrointestinal side effects of 5-FU. However, further studies are necessary to critically evaluate the overall benefits of polyamine pathway activation towards improving regeneration capacity versus increasing cancer risk in humans.

Online content

Any methods, additional references, Nature Portfolio reporting summaries, source data, extended data, supplementary information,

References

1. López-Otín, C., Blasco, M. A., Partridge, L., Serrano, M. & Kroemer, G. The hallmarks of aging. *Cell* **153**, 1194–1217 (2013).
2. Barnett, K. et al. Epidemiology of multimorbidity and implications for health care, research, and medical education: a cross-sectional study. *Lancet* **380**, 37–43 (2012).
3. Pentinmikko, N. & Katajisto, P. The role of stem cell niche in intestinal aging. *Mech. Ageing Dev.* **191**, 111330 (2020).
4. Omrani, O. et al. IFNγ–Stat1 axis drives aging-associated loss of intestinal tissue homeostasis and regeneration. *Nat. Commun.* **14**, 6109 (2023).
5. Funk, M. C. et al. Aged intestinal stem cells propagate cell-intrinsic sources of inflammaging in mice. *Dev. Cell* **58**, 2914–2929.e7 (2023).
6. Pentinmikko, N. et al. Notum produced by Paneth cells attenuates regeneration of aged intestinal epithelium. *Nature* **571**, 398–402 (2019).
7. Nalapareddy, K. et al. Canonical Wnt signaling ameliorates aging of intestinal stem cells. *Cell Rep.* **18**, 2608–2621 (2017).
8. Smith, C. B., Sun, Y. & Sokoloff, L. Effects of aging on regional rates of cerebral protein synthesis in the Sprague-Dawley rat: examination of the influence of recycling of amino acids derived from protein degradation into the precursor pool. *Neurochem. Int.* **27**, 407–416 (1995).
9. Taylor, R. C. & Dillin, A. Aging as an event of proteostasis collapse. *Cold Spring Harb. Perspect. Biol.* **3**, a004440 (2011).
10. Santra, M., Dill, K. A. & de Graff, A. M. R. Proteostasis collapse is a driver of cell aging and death. *Proc. Natl Acad. Sci. USA* **116**, 22173–22178 (2019).
11. Kennedy, B. K. et al. Geroscience: linking aging to chronic disease. *Cell* **159**, 709–713 (2014).
12. Labbadia, J. & Morimoto, R. I. The biology of proteostasis in aging and disease. *Annu. Rev. Biochem.* **84**, 435–464 (2015).
13. Morimoto, R. I. & Cuervo, A. M. Proteostasis and the aging proteome in health and disease. *J. Gerontol. A Biol. Sci. Med. Sci.* **69**, S33–S38 (2014).
14. Hou, Y. et al. Ageing as a risk factor for neurodegenerative disease. *Nat. Rev. Neurol.* **15**, 565–581 (2019).
15. Vilchez, D., Saez, I. & Dillin, A. The role of protein clearance mechanisms in organismal ageing and age-related diseases. *Nat. Commun.* **5**, 5659 (2014).
16. Kip, A. M. et al. Temporal transcript profiling identifies a role for unfolded protein stress in human gut ischemia–reperfusion injury. *Cell. Mol. Gastroenterol. Hepatol.* **13**, 681–694 (2022).
17. Rodriguez-Fernandez, I. A., Qi, Y. & Jasper, H. Loss of a proteostatic checkpoint in intestinal stem cells contributes to age-related epithelial dysfunction. *Nat. Commun.* **10**, 1050 (2019).
18. Zhang, H. et al. Polyamines control eIF5A hypusination, TFEB translation, and autophagy to reverse B cell senescence. *Mol. Cell* **76**, 110–125.e9 (2019).
19. Madeo, F., Eisenberg, T., Pietrocola, F. & Kroemer, G. Spermidine in health and disease. *Science* **359**, eaan2788 (2018).
20. Schuller, A. P., Wu, C. C.-C., Dever, T. E., Buskirk, A. R. & Green, R. eIF5A functions globally in translation elongation and termination. *Mol. Cell* **66**, 194–205.e5 (2017).
21. Saini, P., Eyler, D. E., Green, R. & Dever, T. E. Hypusine-containing protein eIF5A promotes translation elongation. *Nature* **459**, 118–121 (2009).
22. Allmeroth, K. et al. N^1-acetylspermidine is a determinant of hair follicle stem cell fate. *J. Cell Sci.* **134**, jcs252767 (2021).
23. Park, M. H., Cooper, H. L. & Folk, J. E. Identification of hypusine, an unusual amino acid, in a protein from human lymphocytes and of spermidine as its biosynthetic precursor. *Proc. Natl Acad. Sci. USA* **78**, 2869–2873 (1981).
24. Nakamura, A. et al. Symbiotic polyamine metabolism regulates epithelial proliferation and macrophage differentiation in the colon. *Nat. Commun.* **12**, 2105 (2021).
25. Puleston, D. J. et al. Polyamines and eIF5A hypusination modulate mitochondrial respiration and macrophage activation. *Cell Metab.* **30**, 352–363.e8 (2019).
26. Nishimura, K., Shiina, R., Kashiwagi, K. & Igarashi, K. Decrease in polyamines with aging and their ingestion from food and drink. *J. Biochem.* **139**, 81–90 (2006).
27. Nalapareddy, K., Hassan, A., Sampson, L. L., Zheng, Y. & Geiger, H. Suppression of elevated Cdc42 activity promotes the regenerative potential of aged intestinal stem cells. *iScience* **24**, 102362 (2021).
28. Yilmaz, Ö. H. et al. mTORC1 in the Paneth cell niche couples intestinal stem-cell function to calorie intake. *Nature* **486**, 490–495 (2012).
29. Raffaghello, L. et al. Starvation-dependent differential stress resistance protects normal but not cancer cells against high-dose chemotherapy. *Proc. Natl Acad. Sci. USA* **105**, 8215–8220 (2008).
30. Gebert, N. et al. Region-specific proteome changes of the intestinal epithelium during aging and dietary restriction. *Cell Rep.* **31**, 107565 (2020).
31. Imada, S. et al. Short-term post-fast refeeding enhances intestinal stemness via polyamines. *Nature* **633**, 895–904 (2024).
32. Longley, D. B., Harkin, D. P. & Johnston, P. G. 5-fluorouracil: mechanisms of action and clinical strategies. *Nat. Rev. Cancer* **3**, 330–338 (2003).
33. Therizols, G. et al. Alteration of ribosome function upon 5-fluorouracil treatment favors cancer cell drug-tolerance. *Nat. Commun.* **13**, 173 (2022).
34. Chatterjee, S. et al. Ribosome quality control mechanism mitigates the cytotoxic impacts of ribosome collisions induced by 5-fluorouracil. *Nuc. Acids Res.* **52**, 12534–12548 (2024).
35. Chen, J.-K. et al. An RNA damage response network mediates the lethality of 5-FU in colorectal cancer. *Cell Rep. Med.* **5**, 101778 (2024).
36. Beumer, J. & Clevers, H. Regulation and plasticity of intestinal stem cells during homeostasis and regeneration. *Development* **143**, 3639–3649 (2016).
37. Sprangers, J., Zaalberg, I. C. & Maurice, M. M. Organoid-based modeling of intestinal development, regeneration, and repair. *Cell Death Differ.* **28**, 95–107 (2021).
38. Meran, L., Baulies, A. & Li, V. S. W. Intestinal stem cell niche: the extracellular matrix and cellular components. *Stem Cells Int.* **2017**, 7970385 (2017).
39. Rudnick, D. A. & Davidson, N. O. Functional relationships between lipid metabolism and liver regeneration. *Int. J. Hepatol.* **2012**, 549241 (2012).
40. Kwon, S. J., Khan, M. S. & Kim, S. G. Intestinal inflammation and regeneration–interdigitating processes controlled by dietary lipids in inflammatory bowel disease. *Int. J. Mol. Sci.* **25**, 1311 (2024).
41. Hageman, J. H. et al. Intestinal regeneration: regulation by the microenvironment. *Dev. Cell* **54**, 435–446 (2020).
42. Hidalgo-Garcia, L. et al. Intestinal mesenchymal cells regulate immune responses and promote epithelial regeneration in vitro and in dextran sulfate sodium-induced experimental colitis in mice. *Acta Physiol.* **233**, e13699 (2021).
43. Kang, J. et al. Depletion of SAM leading to loss of heterochromatin drives muscle stem cell ageing. *Nat. Metab.* **6**, 153–168 (2024).

44. Gobert, A. P. et al. Hypusination maintains intestinal homeostasis and prevents colitis and carcinogenesis by enhancing aldehyde detoxification. *Gastroenterology* **165**, 656–669.e8 (2023).

45. Gobert, A. P. et al. Protective role of spermidine in colitis and colon carcinogenesis. *Gastroenterology* **162**, 813–827.e8 (2022).

46. Dupont, S. et al. Role of YAP/TAZ in mechanotransduction. *Nature* **474**, 179–183 (2011).

47. Yui, S. et al. YAP/TAZ-dependent reprogramming of colonic epithelium links ECM remodeling to tissue regeneration. *Cell Stem Cell* **22**, 35–49.e7 (2018).

48. Serra, D. et al. Self-organization and symmetry breaking in intestinal organoid development. *Nature* **569**, 66–72 (2019).

49. Lukonin, I. et al. Phenotypic landscape of intestinal organoid regeneration. *Nature* **586**, 275–280 (2020).

50. Poulin, R., Lu, L., Ackermann, B., Bey, P. & Pegg, A. E. Mechanism of the irreversible inactivation of mouse ornithine decarboxylase by alpha-difluoromethylornithine. Characterization of sequences at the inhibitor and coenzyme binding sites. *J. Biol. Chem.* **267**, 150–158 (1992).

51. Gobert, A. P. et al. Protective role of arginase in a mouse model of colitis. *J. Immunol.* **173**, 2109–2117 (2004).

52. Dellorusso, P. V. et al. Autophagy counters inflammation-driven glycolytic impairment in aging hematopoietic stem cells. *Cell Stem Cell* **31**, 1020–1037.e9 (2024).

53. Ripa, R. et al. Refeeding-associated AMPK complex activity is a hallmark of health and longevity. *Nat. Aging* **3**, 1544–1560 (2023).

54. Jardé, T. et al. Mesenchymal niche-derived neuregulin-1 drives intestinal stem cell proliferation and regeneration of damaged epithelium. *Cell Stem Cell* **27**, 646–662.e7 (2020).

55. Hofer, S. J. et al. Mechanisms of spermidine-induced autophagy and geroprotection. *Nat. Aging* **2**, 1112–1129 (2022).

56. Yue, F. et al. Spermidine prolongs lifespan and prevents liver fibrosis and hepatocellular carcinoma by activating MAP1S-mediated autophagy. *Cancer Res.* **77**, 2938–2951 (2017).

57. Fritsch, S. D. et al. Metabolic support by macrophages sustains colonic epithelial homeostasis. *Cell Metab.* **35**, 1931–1943.e8 (2023).

58. Chen, H. et al. Urea cycle activation triggered by host-microbiota maladaptation driving colorectal tumorigenesis. *Cell Metab.* **35**, 651–666.e7 (2023).

59. Kreul, S. M. et al. A phase III skin cancer chemoprevention study of DFMO: long-term follow-up of skin cancer events and toxicity. *Cancer Prev. Res.* **5**, 1368–1374 (2012).

60. Simoneau, A. R. et al. The effect of difluoromethylornithine on decreasing prostate size and polyamines in men: results of a year-long phase IIb randomized placebo-controlled chemoprevention trial. *Cancer Epidemiol. Biomark. Prev.* **17**, 292–299 (2008).

61. Levin, V. A. et al. Phase I–II study of eflornithine and mitoguazone combined in the treatment of recurrent primary brain tumors. *Cancer Treat. Rep.* **71**, 459–464 (1987).

62. Brandhorst, S. et al. A periodic diet that mimics fasting promotes multi-system regeneration, enhanced cognitive performance, and healthspan. *Cell Metab.* **22**, 86–99 (2015).

63. Longo, V. D., Di Tano, M., Mattson, M. P. & Guidi, N. Intermittent and periodic fasting, longevity and disease. *Nat. Aging* **1**, 47–59 (2021).

64. Rangan, P. et al. Fasting-mimicking diet modulates microbiota and promotes intestinal regeneration to reduce inflammatory bowel disease pathology. *Cell Rep.* **26**, 2704–2719.e6 (2019).

65. Sarkar, A. et al. Intermittent fasting induces rapid hepatocyte proliferation to restore the hepatostat in the mouse liver. *eLife* **12**, e82311 (2023).

66. Jensen, L. J. et al. STRING 8—a global view on proteins and their functional interactions in 630 organisms. *Nucleic Acids Res.* **37**, D412–D416 (2009).

[1]Leibniz Institute on Aging—Fritz Lipmann Institute, Jena, Germany. [2]Institute of Pathology, Section of Pediatric Pathology, University Hospital Bonn, Bonn, Germany. [3]Department of Dermatology, University Hospital Essen and German Cancer Consortium, Essen, Germany. [4]Department of Biology, The David H. Koch Institute for Integrative Cancer Research at MIT, MIT, Cambridge, MA, USA. [5]Applied Analytical Chemistry, University of Duisburg-Essen, Essen, Germany. [6]Institute of Molecular Cell Biology, Center for Molecular Biomedicine, Jena University Hospital, Jena, Germany. [7]Broad Institute of Harvard and MIT, Cambridge, MA, USA. [8]Department of Pathology, Beth Israel Deaconess Medical Center and Massachusetts General Hospital and Harvard Medical School, Boston, MA, USA. [9]Department of Life Sciences and Systems Biology, University of Turin, Turin, Italy. [10]Molecular Biotechnology Center, University of Turin, Turin, Italy. [11]Present address: Institute of Biotechnology, Department of Technical Immunology, Technical University Berlin, Berlin, Germany. [12]Present address: Genentech Inc., San Francisco, CA, USA. [13]These authors contributed equally: Alberto Minetti, Omid Omrani. ✉e-mail: francesco.neri@unito.it; alessandro.ori@leibniz-fli.de

Methods

All the experiments were conducted in compliance with relevant ethical regulations. The mouse experiments were conducted according to protocols approved by the state government of Thuringia authority (Thüringer Landesamt für Verbraucherschutz, TLV license number: FLI-20-003) or by the Committee on Animal Care protocol at MIT (protocol number: 2210000430).

Mice

Young (3–5 months old) and old (22–29 months old) WT C57BL6/J mice were obtained from Janvier or from internal breeding at the Leibniz Institute on Ageing–Fritz Lipmann Institute (FLI). They were group-housed and maintained in a specific opportunistic pathogen-free animal facility in FLI with 12 h of light–dark cycle and fed with a standard mouse chow at a temperature of $20 \pm 2\ ^{\circ}C$, relative humidity $55\% \pm 15\%$.

Young (2–4 months) $Odc1^{loxp/loxp}$; $Villin\text{-}CreERT2$ and $Odc1^{wt/wt}$; $Villin\text{-}CreERT2$ mice were generated by crossing $Odc1^{loxp/loxp}$ mice to $Villin\text{-}CreERT2$ mice, which were under the husbandry care of the Department of Comparative Medicine in the Koch Institute for Integrative Cancer Research.

In vivo treatments

For the 5-FU treatment, 5-FU (Sigma-Aldrich no. F6627) was solubilized in PBS (Sigma-Aldrich no. D8537-100ML) at a concentration of 20 mg ml^{-1}. The young and old mice were injected intraperitoneally with 150 mg kg^{-1} of 5-FU (100 mg kg^{-1} for 5-FU before DFMO or PBS experiments) or PBS as control (single injection in the morning). The mice were killed, and the intestinal tissue was collected at the timepoints indicated in the figures for downstream analysis. For the TAM treatment, TAM was administered via intraperitoneal injection suspended in sunflower seed oil (Spectrum S1929) at a concentration of 4 mg ml^{-1} or 10 mg ml^{-1}. $Odc1^{loxp/loxp}$; $Villin\text{-}CreERT2$ and $Odc1^{wt/wt}$; $Villin\text{-}CreERT2$ mice were injected with 2.5 mg per 25 g of TAM every other day (day 1, 3 and 5); 5-FU or PBS was then injected 1 week after the last TAM injection. For the CHX treatments, CHX (Millipore Sigma no. C7698) was suspended in PBS at a concentration of 5 mg ml^{-1}. CHX or PBS (vehicle control) was administered via intraperitoneal injection at a dose of 15 mg kg^{-1}, at the timepoints indicated in the figures. For the DL-a-DFMO treatments, DFMO (Cayman no. 16889) reconstituted in PBS at a concentration of 10 mg ml^{-1} or PBS-vehicle control were administered via intraperitoneal injection at a dose of 200 mg kg^{-1} on 18-month-old mice at the timepoints indicated in the figures. Polyamines supplementation treatments: an equimolar 1:1 ratio of spermidine (Millipore Sigma no. 85580) + spermine (Millipore Sigma no. 3256) resuspended in PBS at a concentration of 5 mg ml^{-1} or PBS as vehicle control were administered via oral gavage at a dose of 45 mg kg^{-1} of total polyamines at the timepoints indicated in the figures.

DR and RF mice experiment

Mice were single-caged 2 weeks before the start of dietary treatment, during which their individual food intake was recorded. These measurements were then used to determine 70% of each mouse's daily food intake, which was applied throughout the DR period. During the DR period, food was given in the morning, once per day for 1 month. The AL animals had unlimited access to food throughout the experiment. The animals of the DR + RF cohort underwent the same dietary treatment as DR animals and received unlimited access to food for 2 days before injection. The mice were then injected intraperitoneally with 5-FU (150 mg kg^{-1}) or PBS as vehicle control in the morning, and unlimited food access was provided after injection to all of the cohorts until the end of experiments.

Hematoxylin and eosin staining

The 5-µm paraffin sections were deparaffinized by washing twice in xylene for 5 min each, followed by rehydration through a graded ethanol series (100%, 90%, 70%, 50% and 30%) for 5 min each and finally rinsed with Milli-Q water for 10 min. The sections were stained in haematoxylin for 3 min, washed in water for 5 min and stained in eosin for 3 min. The sections were then dehydrated through 30%, 50%, 70%, 90% and 100% ethanol and incubated in xylene twice for 5 min each. The slides were mounted by using a xylene-based mounting medium, Depex (VWR no. 100503-836). The section cutting and staining was done by the core FLI histology facility. The images of stained sections were acquired using Axio Imager (Zeiss) and analysed using ZEN blue software v2 (Zeiss). For further image analysis, the graphics tools for counting and measuring the ZEN software were used.

Immunofluorescence and IHC on paraffin-embedded tissue sections

The 5-µm paraffin sections were deparaffinized by two times immersion in xylene (5 min each time) and rehydrated by immersion in a series of graded ethanol dilutions 100%, 90% and 70% for 5 min each. The epitope retrieval was performed by preheating the sections 5 min at full-power microwave (900 W) in 10 mM sodium citrate buffer pH 6.5 until boiling, followed by 10 min at a subboiling temperature (600 W). The sections were cooled down for 20 min, washed in PBS and blocked with 5% bovine serum albumin (BSA) in PBS for 1 h at room temperature in a humid chamber. For the immunofluorescence experiments, the sections were stained with rabbit anti-pH3 (Ser10) (Cell Signaling Technologies no. 9701) (1:100) in 1% BSA in PBS for 16 h at 4 °C in a humid chamber. This was followed by washing in 0.1% Tween 20 in PBS (v/v, 3×, 5 min) and subsequent incubation for 30 min with secondary anti-rabbit IgG conjugated with AF594 (1:1,000). The slides were then washed in 0.1% Tween 20 in PBS 3×, 5 min and mounted with a mounting medium, including 4′,6-diamidino-2-phenylindole. For immunohistochemistry (IHC) experiments, rabbit monoclonal anti-pH3 (Ser10) (Cell Signaling Technologies no. 3377) antibody was used at 1:500, followed by a biotin-conjugated donkey anti-rabbit secondary antibody (1:500, Jackson ImmunoResearch, no. 711-066-152); the antibodies used were diluted in Signal Stain Antibody Diluent (Cell Signaling Technologies). Images were then acquired using Axio Imager (Zeiss) and analysed using ZEN blue software v2 (Zeiss). For further image analysis, the graphics tools for counting and measuring the ZEN software were used.

Small intestinal crypts isolation

After killing the mice with CO_2, the small intestine was isolated and cleaned with cold PBS. The villi were removed by scraping with glass coverslip, and the villi-free intestinal pieces (2 cm) were washed with cold PBS and incubated in 5 mM ethylenediaminetetraacetic acid (EDTA) in PBS for 30–40 min at 4 °C on a rotator. The tissue was transferred to a new 50-ml Falcon filled with fresh cold PBS and manually shaken for 30 s. The crypt solution was filtered using a 70-µm cell strainer (Corning no. 431751) and centrifuged at 450g for 5 min at 4 °C. The isolated crypts were immediately used or snap-frozen in liquid nitrogen and stored at −80 °C for further experiments.

Organoids culture, polyamine-free basal medium and in vitro 5-FU treatment

Small intestine crypts were isolated from mice, as described above. The freshly isolated intestinal crypts were then embedded in 70% v/v Matrigel Growth Factor Reduced (Corning no. 356231) mixed with complete organoid medium. Organoid medium consists of Advanced Dulbecco's modified Eagle medium F12 (Life Technologies no. 12634-010) supplemented with Noggin 100 ng ml^{-1} (Peprotech no. 250-38), recombinant epidermal growth factor 50 ng ml^{-1} (Peprotech no. 315-09), R-spondin 1 mg ml^{-1} (home-made), N2 1× (Life Technologies no. 17502048), B27 1× (Life Technologies no. 12587010), 1× GlutaMax (Thermo Fisher scientific no. 35050061), 10 mM HEPES (Thermo Fisher scientific no. 15630080) and 0.5 U ml^{-1} penicillin–streptomycin (Thermo Fisher Scientific no. 15140122). As for organoids in

polyamine-free basal medium experiments, N2 (putrescine content 10 mM) and B27 (putrescine HCl content n/a) components were removed from the previously described organoids medium and replaced with Y27632 (10uM) and CHIR99021 (2.5UM) to sustain organoids growth. Next, the crypts were plated onto a flat-bottom 24-well plate (VWR no. 734-2325) for 10 min in a 37 °C incubator with 5% CO_2 until the Matrigel solidified. The Matrigel crypt domes were then overlaid with 500 ml organoid medium, which was changed every 3 days. For the in vitro 5-FU treatment, the organoids were allowed to grow for a week after the initial passage and then treated with the reported concentrations of 5-FU solubilized in PBS at a concentration of 20 mg ml^{-1}; 24 h after, the organoids were passaged 1:1 into new plates and collected/analysed at the indicated timepoints.

Annexin V assay

The intestinal organoids were dissociated to single cells by resuspending them in 1 ml of single-cell isolation solution (TrypLE supplemented with 1 mg ml^{-1} DNase I, 5 mM $MgCl_2$, 80 µM Y27632) and incubated for 20 min at 37 °C with short vortexing after first 10 min of incubation. The reaction was quenched by the addition of 29 ml of ice-cold PBS, and the cells were centrifuged at 800g for 5 min at 4 °C. The cell pellet was resuspended in fluorescence-activated cell sorting (FACS) staining media (PBS + fetal bovine serum 2% + EDTA 2.5 uM) supplemented with 80 µM Y27632. Single cells from the intestinal organoids were then resuspended in 200 µl of 1× binding buffer and 1 µl of APC annexin V from the apoptosis detection kit from BD Bioscience following incubation at room temperature for 15 min. After washing with 1× binding buffer, the cells were resuspended in 1× binding buffer (100 µl) and analysed using FACSAriaII (BD Biosciences). The sum of early and late apoptotic cells was used for quantification. All data were analysed using FlowJo software.

Protein lysate and immunoblotting

For protein lysate, intestinal crypts or organoids were lysed in radioimmunoprecipitation assay (RIPA) buffer (RIPA buffer: (150 mM sodium chloride (Roth no. P029.2), 1% Triton X-100 (v/v Roth no. 3051.3), 0.5 % sodium deoxycholate (Thermo Fisher no. 89904), 0.1% sodium dodecyl sulfate (SDS) (w/v Sigma-Aldrich no. 75746-250 G), 50 mM Tris (Roth no. 4855.2) pH8)) supplemented with cOmplete, Mini, EDTA-free Protease Inhibitor (Roche no. 11836170001) and with PhosSTOP Phosphatase Inhibitor (Roche no. 4906837001). The samples were then sonicated in a Bioruptor Plus (Diagenode, Belgium) for ten cycles with 1 min ON and 30 s OFF with high intensity at 4 °C and then centrifuged max speed for 5 min. The resulting supernatant was then collected and the proteins quantified using Pierce BCA protein assay kit (Thermo Scientific no. 23225) following the manufacturer's instructions. The protein lysates were then stored at −80 °C before use. For immunoblotting, 10 to 20 µg of protein lysate in 4× loading buffer (1.5 M Tris pH 6.8, 20% (w/v) SDS, 85% (v/v) glycerin, 5% (v/v) β-mercaptoethanol) were denatured at 95 °C and then separated via SDS–polyacrylamide gel electrophoresis on the 4–20% Mini-Protean TGX Gels (Bio-Rad no. 4561096). For molecular weight estimation, 5 µl of Precision Plus Protein Dual Colour standard (Bio-Rad no. 1610374) was applied. The proteins were then transferred using a semi-wet transfer approach into Nitrocellulose blotting membranes (Carl Roth no. 200H.1) using the Trans-Blot Turbo Transfer Starter System (Bio-Rad Laboratories). The membranes were then stained with Ponceau S (Sigma no. P7170-1L) for 5 min on a shaker (Heidolph Duomax 1030), washed with Milli-Q water, imaged on a Molecular Imager ChemiDocTM XRS + Imaging system (Bio-Rad Laboratories) and destained by two washes with PBS and two washes in Tris-buffered saline (TBS, 25 mM Tris, 75 mM NaCl) with 0.5% (v/v) Tween 20 (TBST) for 5 min. After incubation for 5 min in EveryBlot blocking buffer (Bio-Rad Laboratories no. 12010020), the membranes were incubated overnight with the primary antibodies: mouse-puromycin (Millipore Sigma no. MABE343), mouse-actin

(Millipore Sigma no. MAB1501 clone C4), rabbit-ubiquitin linkage specific K48 (Abcam no. ab140601), rabbit-SQSTM1/p62 (Abcam no. ab91526), mouse-S6 ribosomal protein (Cell Signaling Technologies no. 2317), mouse-ubiquitin P4D1 (Santa Cruz Biotechnology no. sc-8017), rabbit-phospho H3 (Cell Signaling Technologies no. 9701), rabbit-hypusinated EIF5A (Millipore Sigma no. ABS1064), mouse-EIF5a (BD Biosciences no. 611977) diluted (1:1,000) in enzyme dilution buffer (0.2% (w/v) BSA, 0.1% (v/v) Tween 20 in PBS) at 4 °C on a tube roller (BioCote Stuart SRT6). The membranes were then washed three times with TBST for 10 min at room temperature and incubated with horseradish peroxidase coupled secondary antibodies (Dako anti-rabbit no. P0448 or anti-mouse no. P0447) at room temperature for 1 h (1:1,500 or 1:2,000 respectively) in enzyme dilution buffer. After three more washes for 10 min in TBST, the chemiluminescent signals were detected using enhanced chemiluminescence (ECL) with Pierce ECL detection kit (Thermo Fisher Scientific no. 32109). The signals were acquired on the Molecular Imager ChemiDocTM XRS + Imaging system and analysed using the Image Lab 6.1 software (Bio-Rad Laboratories). When needed, membranes were stripped using Restore Western Blot Stripping Buffer (Thermo Scientific no. 21059) 10 ml × 30 min, washed three times with TBST, blocked and then reprobed with the other primary antibody.

Protein synthesis assay

To assess the protein synthesis rate, we used puromycin which incorporates at the C-terminus of nascent polypeptide chains. Freshly isolated crypts were incubated at 37 °C with organoids medium including 10 µl ml^{-1} puromycin for 15 min, centrifuged for 5 min and then, resulting pellet was eluted with RIPA buffer containing cOmplete, Mini, EDTA-free Protease Inhibitor (Roche no. 11836170001) and with PhosSTOP Phosphatase Inhibitor (Roche no. 4906837001). For the in vitro protein synthesis assay, the intestinal organoids were collected in PBS and centrifuged for 5 min; the resulting pellet was then incubated with organoids medium supplemented with 10 µg ml^{-1} puromycin (Millipore Sigma no. P8833) for 15 min, centrifuged 5 min and eluted with RIPA buffer supplemented with proteases and phosphatases inhibitors. The uptaken puromycin to the nascent polypeptide was then analysed with immunoblotting using mouse monoclonal anti-puromycin antibody (Millipore Sigma no. MABE343) diluted 1:1,000.

Quantitative real-time PCR

After killing the mice using CO_2, the intestinal tissue was immediately placed in QIAzol Lysis Reagent (Qiagen no. 79306) and stored at −80 °C for RNA isolation. In total, 1 µg of total RNA was used to prepare complementary DNA (cDNA) using iScript cDNA Synthesis Kit (Bio-Rad Laboratories no. 1708891) according to the manufacturer's protocol. The quantitative real-time PCR analysis was performed on a CFX384 Touch Real-Time PCR System (Bio-Rad Laboratories) using SYBR GreenER qPCR SuperMix (Thermo Fisher Scientific no. 11761500). Each reaction was performed in a 9 µl qPCRmix and 1 µl of 1:10 diluted cDNA. The quantitative real-time PCR conditions were 3 min at 95 °C, then 45 cycles of 15 s at 95 °C and 30 s at 61 °C. To obtain the amplicon data, a melting curve analysis was performed after each PCR run. Each sample was analysed in triplicate. The gene expression was determined following the delta Ct method and normalized to beta-actin. The following mouse primers were used: Actb forward 5′-TCTTTGCAGCTCCTTCGTTG-3′, reverse 5′-ACGATGGAGGGGAATACAGC-3′; p62 forward 5′-AGGAT GGGGACTTGGTTGC-3′, reverse 5′-TCACAGATCACATTGGGGTGC-3′.

Sample preparation for MS analysis

In total, 3 cm of intestinal tissues from distal ileum were thawed and transferred into Precellys lysing kit tubes (Keramik-kit 1.4/2.8 mm, 2 ml (CKM)) containing 500 µl of PBS supplemented with 1 tab of cOmplete, Mini, EDTA-free Protease Inhibitor per 50 ml. For homogenization, the tissues were shaken twice at 6,000 rpm for 30 s using Precellys 24 Dual (Bertin Instruments), and the homogenate was transferred

to new 1.5-ml Eppendorf tubes. Based on estimated protein content, 100 µg of protein was processed for small intestine whole proteome and 25 µg for young ODC1 WT/KO mice proteome. The volumes were adjusted using PBS, and one volume equivalent of 2× lysis buffer (100 mM HEPES pH 8.0, 2% (w/v) SDS) was added. The samples were sonicated in a Bioruptor Plus (Diagenode, Belgium) for ten cycles with 1 min ON and 30 s OFF with high intensity at 20 °C. The samples were heated for 10 min at 95 °C, and a second sonication cycle was performed as described above. The samples were reduced using 10 mM dithiothreitol (Roth no. 6908.3) for 30 min at room temperature and alkylated using freshly made 15 mM iodoacetamide (Sigma-Aldrich no. I1149) for 30 min at room temperature in the dark. Subsequently, the proteins were acetone-precipitated and digested using LysC (Wako sequencing grade no. 125-05061) and trypsin (Promega sequencing grade no. V5111), as described by Buczak et al.[67]. The digested proteins were then acidified with 10% (v/v) trifluoroacetic acid and desalted using Waters Oasis HLB µElution Plate 30 µm (Waters no. 186001828BA) following manufacturer instructions. The eluates were dried down using a vacuum concentrator and reconstituted in 5% (v/v) acetonitrile, 0.1% (v/v) formic acid. The samples were transferred to an MS vial, diluted to a concentration of 1 µg µl⁻¹ and spiked with indexed retention time kit peptides (Biognosys AG no. Ki-3002-2) before analysis by LC–tandem MS (MS–MS).

For polyamine supplementation in aged mice experiments, after lysis, 15 µg of each sample were processed using S-traps. In brief, samples were acidified with phosphoric acid (final concentration 2.5%), and seven times the sample volume of S-trap binding buffer was added (100 mM triethylammonium bicarbonate (TEAB), 90% methanol). The samples were bound on a 96-well S-trap micro plate (Protifi) and washed three times with a binding buffer. Trypsin in 50 mM TEAB pH 8.5 was added to the samples (1 µg per sample) and incubated for 1 h at 47 °C. The samples were eluted in three steps with 50 mM TEAB pH 8.5, elution buffer 1 (0.2% formic acid in water) and elution buffer 2 (50% acetonitrile and 0.2% formic acid). The eluates were dried using a speed vacuum centrifuge (Eppendorf Concentrator Plus, Eppendorf AG) and frozen until further analysis.

Proteomics data acquisition

For the intestinal tissues whole proteome, the peptides were separated in trap/elute mode using the nanoAcquity MClass Ultra-High Performance Liquid Chromatography system (Waters) equipped with trapping (nanoAcquity Symmetry C18, 5 µm, 180 µm × 20 mm) and an analytical column (nanoAcquity BEH C18, 1.7 µm, 75 µm × 250 mm). Solvent A was water and 0.1% formic acid, and solvent B was acetonitrile and 0.1% formic acid. In total, 1 µl of the samples (~1 µg on column) were loaded with a constant flow of solvent A at 5 µl min⁻¹ onto the trapping column. The trapping time was 6 min. The peptides were eluted via the analytical column with a constant flow of 0.3 µl min⁻¹. During the elution, the percentage of solvent B increased nonlinearly from 0–40% in 120 min. The total run time was 145 min, including equilibration and conditioning. The LC was coupled to an Orbitrap Exploris 480 (Thermo Fisher Scientific) using the Proxeon nanospray source. The peptides were introduced into the mass spectrometer via a Pico-Tip Emitter 360-µm outer diameter × 20-µm inner diameter, 10-µm tip (New Objective) heated at 300 °C, and a spray voltage of 2.2 kV was applied. The capillary temperature was set at 300 °C. The radio frequency ion funnel was set to 30%. For DIA data acquisition, full scan MS spectra with a mass range 350–1,650 m/z were acquired in profile mode in the Orbitrap with the resolution of 120,000 FWHM. The default charge state was set to 3+. The filling time was set at a maximum of 60 ms with a limitation of 3×10^6 ions. The DIA scans were acquired with 40 mass window segments of differing widths across the MS1 mass range. The higher collisional dissociation fragmentation (stepped normalized collision energy; 25%, 27.5% and 30%) was applied, and MS–MS spectra were acquired with a resolution of 30,000 FWHM with a fixed first mass of

200 m/z after accumulation of 3×10^6 ions or after filling time of 35 ms (whichever occurred first). The data were acquired in profile mode. For data acquisition and processing of the raw data, Xcalibur 4.3 (Thermo Fisher Scientific) and Tune version 2.0 were used.

For the polyamine supplementation in aged mice and young ODC1 WT/KO experiments, the peptides were reconstituted in MS Buffer before analysis (5% acetonitrile, 95% Milli-Q water, with 0.1% formic acid), spiked with indexed retention time peptides (Biognosys) and loaded on Evotips (Evosep) according to the manufacturer's instructions. In short, Evotips were first washed with Evosep buffer B (acetonitrile, 0.1% formic acid), conditioned with 100% isopropanol and equilibrated with Evosep buffer A. Afterwards, the samples were loaded on the Evotips and washed with Evosep buffer A. The loaded Evotips were topped up with buffer A and stored until the measurement.

The peptides were separated using the Evosep One system (Evosep) equipped with a 15 cm × 150 µm inner diameter packed with a 1.5-µm Reprosil-Pur C18 bead column (Evosep performance, EV-1107, PepSep). The samples were run with a preprogrammed proprietary Evosep gradient of 44 min (30 samples per day) using water and 0.1% formic acid and solvent B acetonitrile and 0.1% formic acid as solvents. The LC was coupled to an Orbitrap Exploris 480 (Thermo Fisher Scientific) using PepSep Sprayers and a Proxeon nanospray source. The peptides were introduced into the mass spectrometer via a PepSep Emitter 360-µm outer diameter × 20-µm inner diameter, heated at 300 °C, and a spray voltage of 2 kV was applied. The injection capillary temperature was set at 300 °C. The radio frequency ion funnel was set to 30%. For DIA data acquisition, full scan MS spectra with a mass range of 350–1,650 m/z were acquired in profile mode in the Orbitrap with a resolution of 120,000 FWHM. The default charge state was set to 2+, and the filling time was set at a maximum of 20 ms with a limitation of 3×10^6 ions. DIA scans were acquired with 40 mass window segments of differing widths across the MS1 mass range. Higher collisional dissociation fragmentation (normalized collision energy 30%) was applied, and MS–MS spectra were acquired with a resolution of 30,000 FWHM with a fixed first mass of 200 m/z after accumulation of 1×10^6 ions or after filling time of 45 ms (whichever occurred first). The data were acquired in profile mode. For data acquisition and processing of the raw data, Xcalibur 4.4 (Thermo) and Tune version 4.0 were used.

Proteomics data analysis

For the small intestine whole proteome, the DIA were searched against a spectral library generated using Spectronaut Professional v15.4 (Biognosys AG). For the library creation, the DDA and DIA raw files were searched with Pulsar (Biognosys AG) against the mouse UniProt database (*Mus musculus*, v. 160106, 16,747 entries) with a list of common contaminants (247 entries) appended, using the default settings. The library contained 101,920 precursors and 6,569 protein groups satisfying an false discovery rate of 1% at both the precursor and protein group level.

The DIA data were searched against this spectral library using Spectronaut Professional v.16.0 and default settings. The protein quantification was performed in Spectronaut using default settings, except: protein LFQ method = QUANT 2.0; proteotypicity filter = only protein group specific; major group quantity = median peptide quantity; major group top N = OFF; minor group quantity = median precursor quantity; minor group top N = OFF; data filtering = Q value sparse; normalization strategy = local normalization; row selection = automatic. The data (report table) were then exported, and further data analyses and visualization were performed with Rstudio using in-house pipelines and scripts.

For polyamine supplementation in aged mice and young ODC1 WT/KO mice proteome analyses, the data were analysed using direct-DIA with Spectronaut v.19 using the above mentioned databases. In addition, the parameters were the same as above. The tests for differential abundance were performed using an unpaired t-test between replicates. The P values were corrected for multiple testing using the

method described by Storey to obtain false discovery rate-adjusted P values (q values)[68].

Clustering and comparison of young and old protein abundance profiles

The normalized protein quantities for the regeneration time course were filtered for protein groups quantified by at least two unique (proteotypic) peptides. All of the timepoints post 5-FU (2 days, 5 days and 7 days) were compared with the median of PBS-injected control samples, and protein groups that showed an absolute $\log_2$ fold change >0.5 at any timepoint were selected for clustering analysis. The determination of an optimal number of clusters, clustering and REACTOME pathway enrichment analysis for each cluster was performed with ClueR[69] using the $\log_2$ fold change to PBS as input.

For the comparison of young and old mice, the ratios to PBS control from individual replicates were $\log_2$ transformed, and the missing values were removed. The protein abundance profiles were compared using MANOVA by setting protein ratios at different timepoints as dependent variables and age group as treatment.

Polyamines measurement

Chemicals. Ultrapure and desalted water with a resistivity of 18.2 M Ω cm^{-1} was generated by a Sartorius Stedim water purification system (Sartorius). All the chemicals used for polyamines and amino acids measurement are presented in Supplementary Table 5 (chemicals used for polyamines and amino acids measurement).

Extraction of amino acids and polyamines. The polyamines were extracted by a two-step liquid extraction adapted from Sellik et al. 2011[70]. In brief, 50,000 crypts were snap-frozen in liquid nitrogen for quenching. The frozen crypts were extracted by adding 500 µl pre-chilled methanol (−80 °C), 20 µl of internal standard (L-arginine-$^{13}C_6$, spermidine-$^2H_6$ and spermine-$^2H_8$ at a concentration of 100 µM which will result in a concentration of 10 µM in the final extract) and vortexed for 2 min until no cell clumps were visible. Afterwards, the samples were sonicated in a chilled (0 °C) ultrasonic bath for 2 min. The cells were kept at −80 °C for 5 min and subsequently thawed. The thawed cells were vortexed and sonicated for 2 min and centrifuged at 3,000g for 5 min. The supernatant was collected and 250 µl of water acidified with 0.1 % acetic acid (liquid chromatography–MS (LC–MS) grade) was added. The samples were vortexed and sonicated for 2 min and subject to the same freezing–thawing cycle described before. The thaw samples were again vortex and sonicated for 2 min, respectively. Next, the samples were centrifuged at 3,000g for 5 min and the supernatant was collected. The combined supernatant was dried in a vacuum centrifuge for 45 min until complete dryness. The dried extract was resuspended in 200 µl acetonitrile/water (60/50; v/v) by sonicating and vortexing for 2 min, respectively. The final extract was obtained as the supernatant following a final centrifugation at 12,000 rpm for 2 min.

Dansylation of polyamines. Dansylation was carried out by using 80 µl of the obtained extract or of a standard solution with a known concentration. The solution is dried and then reconstituted in 80 µl water, 40 µl PBS (1×) and 20 µl of 1 M NaOH. The reaction was started by adding 80 µl of a dansylchloride solution (10 mg ml^{-1} in acetone). The mixture was incubated at 55 °C for 30 min. Afterwards, the solution was dried in a vacuum centrifuge to complete dryness for 45 min. The residue was dissolved in 80 µl of acetonitrile/water (50/50; v/v) and subsequently analysed by LC–MS.

LC–MS analysis and quantification of small molecules. For polyamine analysis, an Agilent 1290 Infinity LC system coupled to an Agilent 6470 QqQ-MS was used (Agilent Technologies). The liquid chromatographic separation was carried out using a Zorbax Eclipse Plus C18 RRHD (50 mm × 2.1 mm, 1.8 µm; Agilent Technologies). The elution

was carried out by utilizing a gradient at a flow rate of 400 µl min^{-1} with water (10 mM ammonium formate pH 3.5) as solvent A and acetonitrile in water (90/10; v/v; 10 mM ammonium formate pH 3.5) as solvent B. The linear gradient was: 0 min, 15% B; 2 min, 15% B; 7 min, 100% B; 10 min, 100% B followed by 2 min at initial condition for re-equilibration. The column temperature was 45 °C, and the injection volume was 10 µl. Ionization was carried out in electrospray-positive mode by using the Agilent jet stream source. The following MS parameters were used: capillary 4,500 V, nozzle voltage 1,000 V, gas temperature 275 °C, gas flow 10 l min^{-1}, nebulizer gas pressure 25 psi, sheath gas temperature 350 °C and sheath gas flow 10 l min^{-1}. The detection was carried out in selected reaction monitoring using the following optimized transitions for the transitions and parameters shown in Supplementary Table 5 (transition settings and internal standards for the analysis of polyamines). For the amino acid analysis, the same system was used. The liquid chromatographic separation was carried out using a AdvanceBio MS Spent Media HILIC column (2.1 mm × 150 mm 2.7 µm; Agilent Technologies). For elution, a binary gradient with water 10 mM ammonium formate + 0.1% formic acid as A and 90/10 ACN/water 10 mM ammonium formate + 0.1% formic acid as B was used. The flow rate was 400 µl, and the linear gradient programme was: 0 min 90% B, 2 min 90% B, 12 min 40% B and 12.1 min 5% B, which was held for 6 min followed by 4 min at initial conditions for re-equilibration. The column temperature was 45 °C, and the injection volume was 10 µl. For electrospray and MS detection the following parameters were used: capillary 3,000 V, nozzle voltage 0 V, gas temp. 225 °C, gas flow 6 l min^{-1}, nebulizer gas pressure 40 psi, sheath gas temp. 225 °C, sheath gas flow 10 l min^{-1}. The detection was carried out in selected reaction monitoring using the following optimized transitions for the transitions and parameters shown in Supplementary Table 5 (transition settings and internal standards for the analysis of amino acids). The non-derivatized polyamines were only monitored with this method, but spermidine and spermine showed a rather high limit-of-detections. Therefore, the quantification of these compounds was done in a separate method.

The quantification in crypt cells was performed by an external calibration in a range from 0.1 µM to 90 µM using three deuterated internal standards (L-arginine-$^{13}C_6$, spermidine-$^2H_6$ and spermine-$^2H_8$) at a concentration of 10 µM. For calibration, the analyte to internal standard area ratios were linearly fitted to the corresponding concentration ratios and compared with the area ratios detected in the samples.

Statistics and reproducibility

The body weight profiles and bar plots from morphological analysis, immunoblot quantifications and FACS-based analysis, were generated using GrapPad Prism 10.0.3 for data visualization and statistics. The data in graphs are shown as mean ± s.d. All the applied statistical tests are listed in the relative figure legends. The protein profiles from proteomics, correlation analyses, scatter plots and volcano plots were generated in R using the ggplot2 package, with statistical analyses specified in the respective figure legend. See 'Proteomics data analysis' section for additional details of proteomic data analysis.

The sample size was not predetermined by statistical methods but was estimated from preliminary experiments, aiming for a minimum of $n = 3$ per group, which was sufficient to reproducibly detect statistically significant differences. The data distribution was assumed to be normal, but this was not formally tested. Aged-matched and sex-matched mice were randomly assigned, ensuring equal distribution among groups. The investigators were not blinded to allocation during experiments and outcome assessment. All experimental replications yielded comparable outcomes. All sample numbers (n) represent biological replicates, with no samples or animals excluded from analysis.

Reporting summary

Further information on research design is available in the Nature Portfolio Reporting Summary linked to this article.

Data availability

Key resource information is available in Supplementary Table 6. Details for light microscopy data acquisition are reported in Supplementary Table 7. The MS-based proteomics data presented in this study are deposited in the MassIVE database under accession no. MSV000094212 (small intestine whole proteome), MSV000098282 (polyamines supplementation in aged mice proteome) and MSV000098281 (young ODC1 WT/KO mice proteome). All other data supporting the findings of this study are available from the corresponding author on reasonable request. Source data are provided with this paper.

References

67. Buczak, K. et al. Spatially resolved analysis of FFPE tissue proteomes by quantitative mass spectrometry. *Nat. Protoc.* **15**, 2956–2979 (2020).
68. Storey, J. D. A direct approach to false discovery rates. *J. R. Stat. Soc. Ser. B* **64**, 479–498 (2002).
69. Yang, P. et al. Knowledge-based analysis for detecting key signaling events from time-series phosphoproteomics data. *PLoS Comput. Biol.* **11**, e1004403 (2015).
70. Sellick, C. A., Hansen, R., Stephens, G. M., Goodacre, R. & Dickson, A. J. Metabolite extraction from suspension-cultured mammalian cells for global metabolite profiling. *Nat. Protoc.* **6**, 1241–1249 (2011).

Acknowledgements

Author contributions

Conceptualization: A.M., A.O., A.T., C.B., F.N., N.G., O.O., Ö.Y. Data curation: A.M., A.O., A.T., C.B., J.L., M.R., O.O. Investigation: A.M., A.T., C.B., G.A., F.C., I.H., J.R., K.S., N.R., O.O., S.I., S.K. Methodology: A.M., A.T., C.B., E.C., O.O., S.W.M. Project administration: A.O., F.N. Data analysis: A.M., A.O., A.T., C.B., O.O. Supervision: A.O., A.T., F.N., R.H., Ö.Y. Visualization: A.M., A.O., C.B., O.O. Writing—original draft: A.M., A.O., C.B., O.O. Writing—review and editing: A.T., F.N. Both A.M. and O.O. contributed equally and have the right to list their name first in their CV.

Competing interests

The authors declare no competing interests.

Additional information

Extended data is available for this paper at https://doi.org/10.1038/s41556-025-01804-9.

Supplementary information The online version contains supplementary material available at https://doi.org/10.1038/s41556-025-01804-9.

Correspondence and requests for materials should be addressed to Francesco Neri or Alessandro Ori.

Peer review information *Nature Cell Biology* thanks Ophir Klein, Keith Wilson and the other, anonymous, reviewer(s) for their contribution to the peer review of this work. Peer reviewer reports are available.

Reprints and permissions information is available at www.nature.com/reprints.
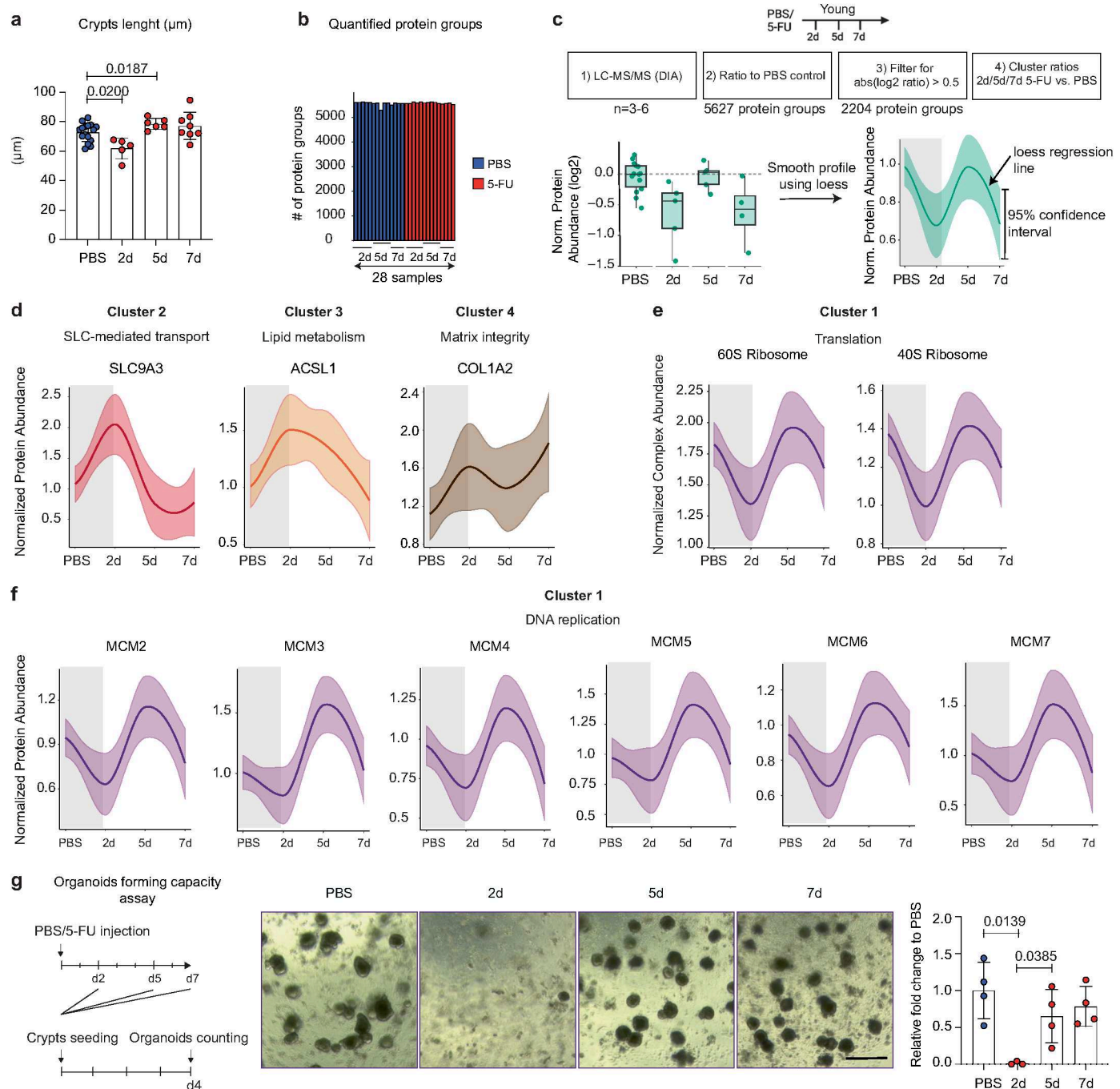
Extended Data Fig. 1 | Proteome dynamics during young small intestinal epithelium regeneration. a Quantification of crypt length in the indicated groups. PBS-treated mice from different days were combined. Each dot represents one mouse. $n = 16$ PBS, $n = 5$ day 2, $n = 6$ day 5, $n = 8$ day 7 5-FU. Data are presented as mean ± SD. p-value was calculated using two-tailed Welch's t test. **b** Number of quantified protein groups in the indicated treatments and time points. PBS-treated young mice: $n = 5$ day 2, $n = 5$ day 5, $n = 4$ day 7. 5-FU-treated young mice: $n = 5$ day 2, $n = 5$ day 5, $n = 4$ day 7. **c** Schematic of experimental design, proteomics data analysis and visualization strategy. **d** Representative abundance profiles for proteins affected by 5-FU treatment and belonging to different clusters. Protein profiles are plotted using a loess smooth function. The shaded area around the regression line represents the 95% confidence interval. $n = 14$ PBS, $n = 5$ day 2, $n = 5$ day 5, $n = 4$ day 7 5-FU. **e** Protein abundance

profiles of 40S (26 proteins) and 60S (41 proteins) ribosome complexes. Protein profiles are plotted using a loess smooth function. The shaded area around the regression line represents the 95% confidence interval. $n = 14$ PBS, $n = 5$ day 2, $n = 5$ day 5, $n = 4$ day 7 5-FU. **f** Protein abundance profiles of components of the MCM complex. Protein profiles are plotted using a loess smooth function. The shaded area around the regression line represents the 95% confidence interval. $n = 14$ PBS, $n = 5$ day 2, $n = 5$ day 5, $n = 4$ day 7 5-FU. **g** Left: Schematic of colony forming assay. Middle: Representative pictures of organoids in the different groups. Right: quantification of the growing organoids in the indicated groups normalized to the average of PBS, scale bar, 200 μm. $n = 4$ PBS; $n = 3$ day 2, $n = 4$ day 5, $n = 4$ day 7 5-FU. Data are presented as mean ± SD. p-value was calculated using two-tailed Welch's t-test.
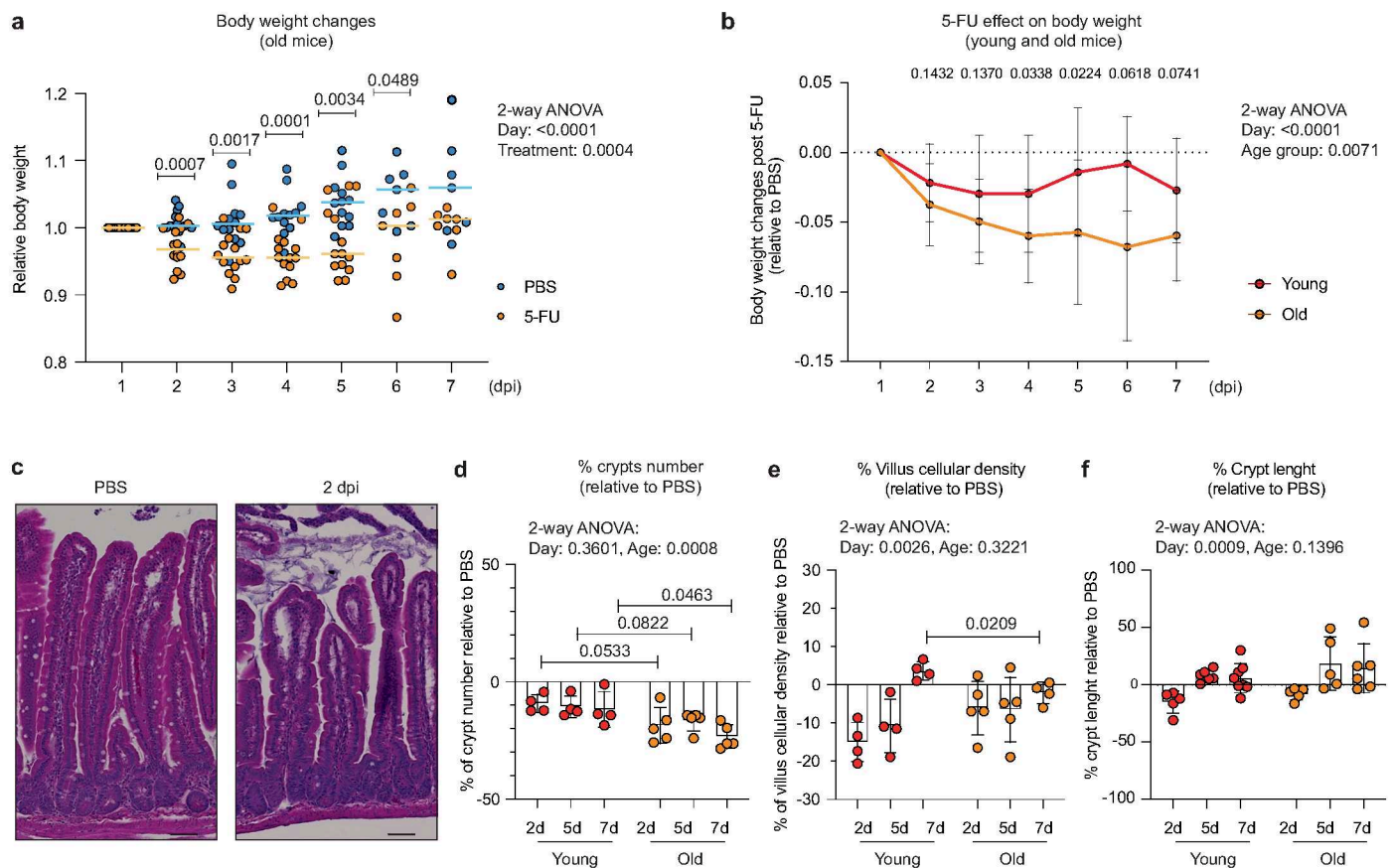
Extended Data Fig. 2 | Old mice show signs of delayed regeneration following 5-FU. a Relative body weight of old mice treated with a single dose of 5-FU or PBS as control. Body weight of each mouse was normalized to its body weight at the day of injection. $n = 12$ PBS, $n = 14$ 5-FU mice. Orange and light blue lines indicate the median body weight for each treatment group on each day. p-values were calculated using two-tailed Welch's t-test by comparing the body weights of 5-FU treated mice with PBS-treated controls on the indicated day, and by two-way ANOVA for overall day and treatment comparisons. **b** Body weight changes of young and old mice after 5-FU. Each mouse's body weight was normalized to its weight on the day of the PBS or 5-FU injection. At each time point, the average body weight change in PBS-treated controls was subtracted from that of 5-FU-treated mice. This analysis isolates the effect of 5-FU on body weight dynamics between young and old groups. (Averages obtained from: $n = 18$ PBS, $n = 17$ 5-FU young mice and $n = 12$ PBS, $n = 14$ 5-FU old mice). Data are presented as mean ± SD. p-values were calculated using two-tailed Welch's t-test and two-way ANOVA. **c** Representative pictures of H&E staining of the aged small intestine

(PBS and 2 dpi). Scale bars, 50 μm. **d** Percentage of crypts number relative to PBS. At each time point 5-FU values were normalized to the average PBS control mice and expressed as percentage. Young mice $n = 4$ per time point; old mice: $n = 5$ per time point. Data are presented as mean ± SD. p-value was calculated using two-tailed Welch's t-test for time point comparison and two-way ANOVA for overall day and age comparisons. **e** Percentage of villus cellular density relative to PBS. At each time point 5-FU values were normalized to the average of PBS and expressed as percentage. Young mice $n = 4$ per time point; old mice: $n = 5$ day 2, $n = 5$ day 5, $n = 4$ day 7. Data are presented as mean ± SD. p-value was calculated using two-tailed Welch's t-test for time point comparison and two-way ANOVA for overall day and age comparisons. **f** Percentage of crypts length relative to PBS. At each time point 5-FU values were normalized to the average of PBS and expressed as percentage. Young mice: $n = 5$ day 2, $n = 6$ day 5, $n = 8$ day 7; old mice: $n = 5$ day 2, $n = 5$ day 5, $n = 6$ day 7. Data are presented as mean ± SD. p-value was calculated using two-way ANOVA for overall day and age comparisons.
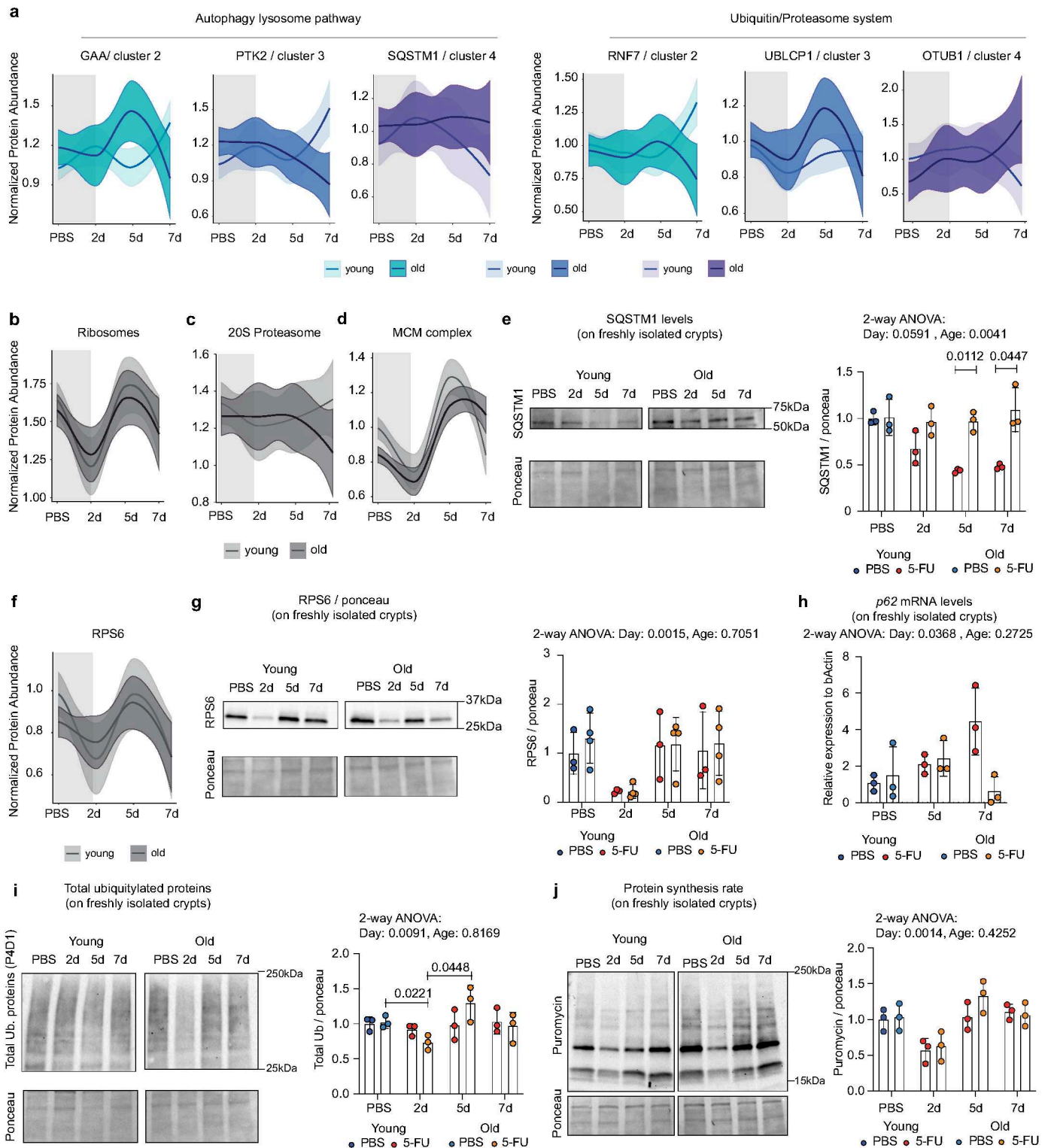
Extended Data Fig. 3 | See next page for caption.

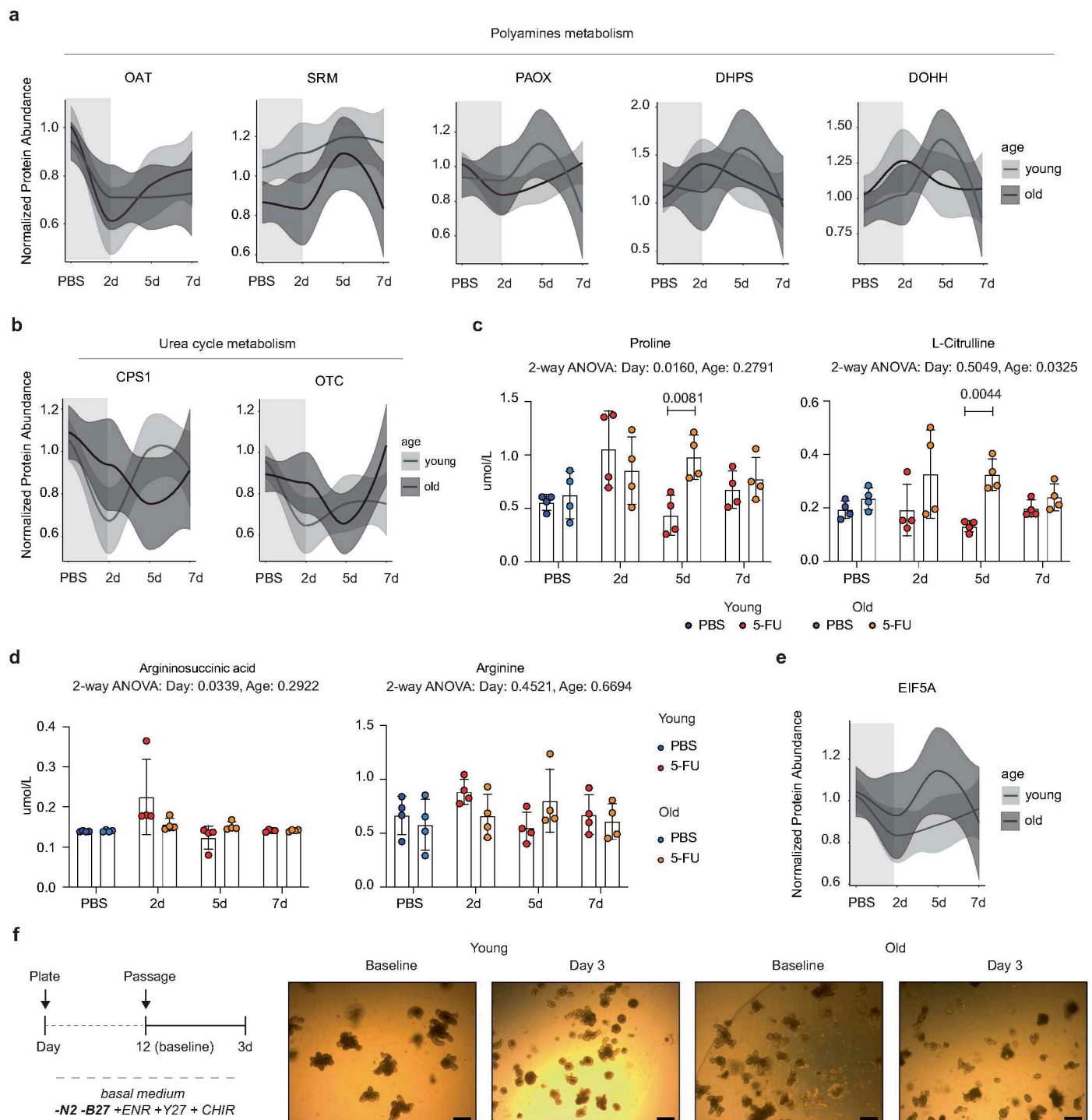**Extended Data Fig. 3 | Perturbation of proteostasis after injury in aged intestinal tissue. a** Left: Protein abundance profiles of the proteins related to the autophagy lysosome pathway. Right: Protein abundance profiles of the ubiquitin proteasome pathway. Proteostasis-related proteins list was obtained from https://www.proteostasisconsortium.com/pn-annotation/. Protein profiles are plotted using a loess smooth function. The shaded area around the regression line represents the 95% confidence interval. $n = 14$ PBS young, $n = 5$ day 2, $n = 5$ day 5, $n = 4$ day 7 5-FU young; $n = 15$ PBS old, $n = 5$ day 2, $n = 5$ day 5, $n = 3$ day 7 5-FU old. **b**–**d** Protein abundance profiles of ribosomal proteins (**b**; 67 proteins), 20S proteasome (**c**; 17 proteins) and MCM complex (**d**; 6 proteins). Protein profiles are plotted using a loess smooth function. The shaded area around the regression line represents the 95% confidence interval. $n = 14$ PBS young, $n = 5$ day 2, $n = 5$ day 5, $n = 4$ day 7 5-FU young; $n = 15$ PBS old, $n = 5$ day 2, $n = 5$ day 5, $n = 3$ day 7 5-FU old. **e** Left: representative immunoblot for the SQSTM1 protein in the indicated groups. Right: Quantification of SQSTM1 protein level relative to ponceau staining (loading control). Each dot represents one mouse. $n = 3$ mice per group. Data are presented as mean ± SD. p-value was calculated using two-tailed Welch's t-test for time point comparison and two-way ANOVA for overall day and age comparisons. **f** Protein abundance profiles of the RPS6 protein. Protein profiles are plotted using a loess smooth function. The shaded area around the regression line represents the 95% confidence interval. $n = 14$ PBS young, $n = 5$ day 2, $n = 5$ day 5, $n = 4$ day 7 5-FU young; $n = 15$ PBS old, $n = 5$ day 2, $n = 5$ day 5, $n = 3$ day 7 5-FU old. **g** Left: representative immunoblot for the RPS6 protein. Right: Quantification of RPS6 protein level relative to ponceau staining (loading control). Each dot represents one mouse. $n = 3$-4 mice per group. Data are presented as mean ± SD. p-value was calculated using Welch's t-test for time point comparison and two-way ANOVA for overall day and age comparisons. **h** Relative mRNA expression level of the *p62* gene in the indicated groups. Data are presented as mean ± SD. p-value was calculated using Welch's t-test for time point comparison and two-way ANOVA for overall day and age comparisons. **i** Left: representative immunoblot for the total ubiquitylated conjugates. Right: Quantification of total ubiquitylated proteins relative to ponceau staining (loading control). Each dot represents one mouse. $n = 3$ mice per group. Data are presented as mean ± SD. p-value was calculated using two-tailed Welch's t-test for time point comparison and two-way ANOVA for overall day and age comparisons. **j** Left: Representative immunoblot for the puromycin incorporation. Right: Quantification of puromycin incorporation relative to ponceau staining (loading control). Each dot represents one mouse. $n = 3$ mice per group. Data are presented as mean ± SD. p-value was calculated using two-tailed Welch's t-test for time point comparison and two-way ANOVA for overall day and age comparisons.

a CHX-treated young mice (2-4 mo.) during regeneration (day 4 collection)

b 5-FU injected

c CHX-treatment in young uninjured mice (2-4 mo.)

2-WAY ANOVA: Day: 0.0988; Treatment: 0.5073
Day x Treatment: 0.1351

d Gating strategy for Annexin V assay on regenerating organoids
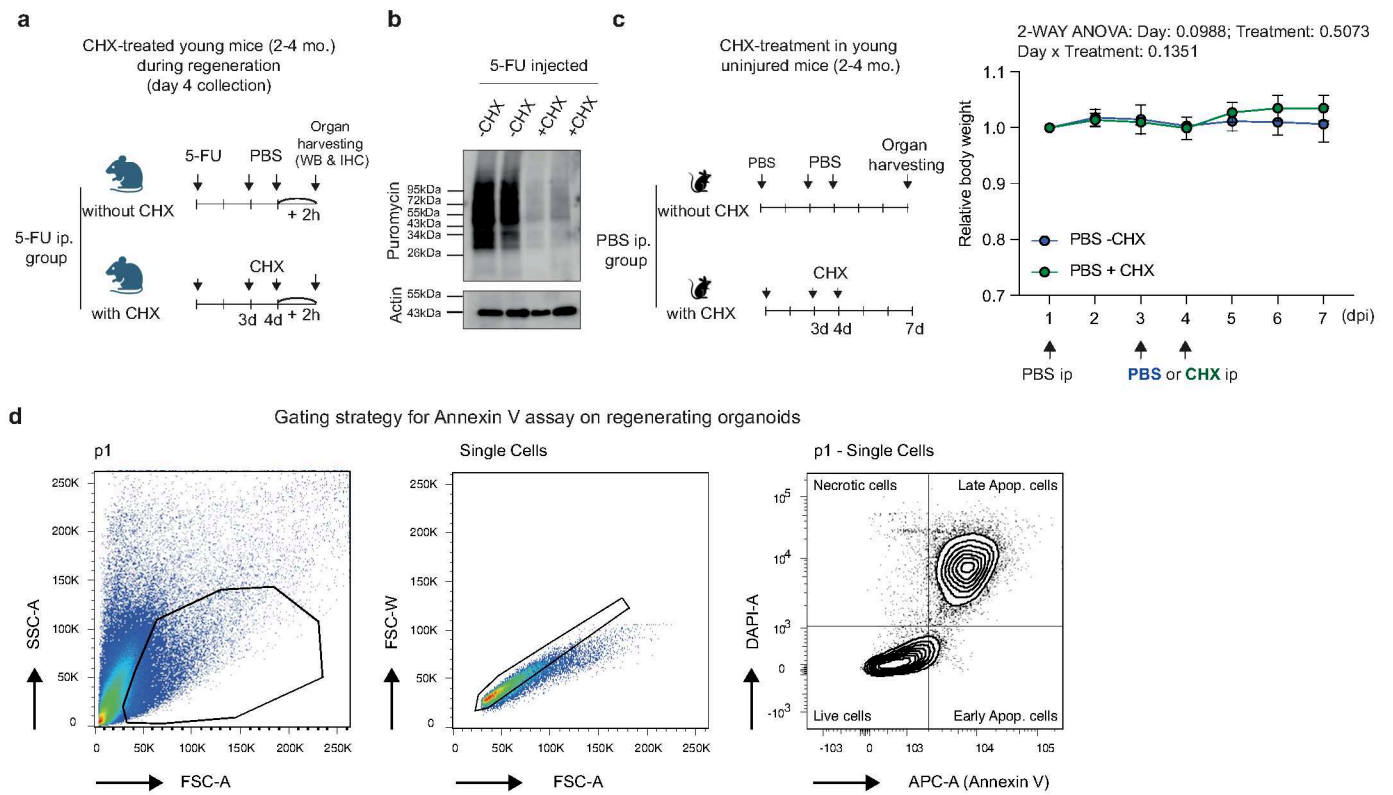
Extended Data Fig. 4 | CHX-induced perturbation of proteostasis in young mice. a Schematic of the effect of CHX on intestinal regeneration in young mice, collection at day 4. **b** Representative immunoblot for puromycin incorporation on 5-FU injected mice (± CHX). **c** Left: Schematic of the effect of CHX on the small intestine of young mice (PBS injected). Right: Relative body weight of young mice treated with a single dose of PBS and injected twice with CHX or PBS as control. Body weight of each mouse was normalized to its body weight at the day of PBS injection (day 1). n = 3 PBS-PBS, n = 3 PBS-CHX young mice. Data are presented as mean ± SD. p-value is calculated with two-way ANOVA for overall group comparisons. **d** FACS gating strategy for annexin V assay used to analyze apoptotic cells in young and old organoids treated with 2.5 µg/ml of 5-FU (related to Fig. 3f). Panel **a** created with BioRender.com.

a

Polyamines metabolism

OAT SRM PAOX DHPS DOHH

age — young — old

b

Urea cycle metabolism

CPS1 OTC

age — young — old

c

Proline
2-way ANOVA: Day: 0.0160, Age: 0.2791

L-Citrulline
2-way ANOVA: Day: 0.5049, Age: 0.0325

Young PBS 5-FU
Old PBS 5-FU

d

Argininosuccinic acid
2-way ANOVA: Day: 0.0339, Age: 0.2922

Arginine
2-way ANOVA: Day: 0.4521, Age: 0.6694

Young PBS 5-FU
Old PBS 5-FU

e

EIF5A

age — young — old

f

Plate Passage

Day 12 (baseline) 3d

basal medium
-N2 -B27 +ENR +Y27 + CHIR

Young Baseline Day 3
Old Baseline Day 3

Extended Data Fig. 5 | Polyamines pathway during intestinal regeneration. a
Protein abundance profiles of the enzymes involved in polyamines biosynthetic pathways. Protein profiles are plotted using a loess smooth function. The shaded area around the regression line represents the 95% confidence interval. $n = 14$ PBS young, $n = 5$ day 2, $n = 5$ day 5, $n = 4$ day 7 5-FU young; $n = 15$ PBS old, $n = 5$ day 2, $n = 5$ day 5, $n = 3$ day 7 5-FU old. **b** Protein abundance profiles of the enzymes involved in urea cycle metabolism. Protein profiles are plotted using a loess smooth function. The shaded area around the regression line represents the 95% confidence interval. $n = 14$ PBS young, $n = 5$ day 2, $n = 5$ day 5, $n = 4$ day 7 5-FU young; $n = 15$ PBS old, $n = 5$ day 2, $n = 5$ day 5, $n = 3$ day 7 5-FU old. **c**, Quantification of proline and L-citrulline. **d** Quantification of arginosuccinic acid and arginine amino acids by LC-MS. Each dot represents one mouse. $n = 4$

mice per condition. Data are presented as mean ± SD. *p*-value was calculated using two-tailed Welch's t-test for time point comparison and two-way ANOVA for overall day and age comparisons. **e** Protein abundance profiles of the Eukaryotic Translation Initiation Factor 5 A (EIF5A). Protein profiles are plotted using a loess smooth function. The shaded area around the regression line represents the 95% confidence interval. $n = 14$ PBS young, $n = 5$ day 2, $n = 5$ day 5, $n = 4$ day 7 5-FU young; $n = 15$ PBS old, $n = 5$ day 2, $n = 5$ day 5, $n = 3$ day 7 5-FU old. **f** Left: Schematic of young and old organoids in polyamines free basal media. On day 12 young and old organoids were passaged to induce regeneration. Right: representative pictures of fully developed organoids before passaging (baseline) and at day 3. Scale bars, 200 µm.
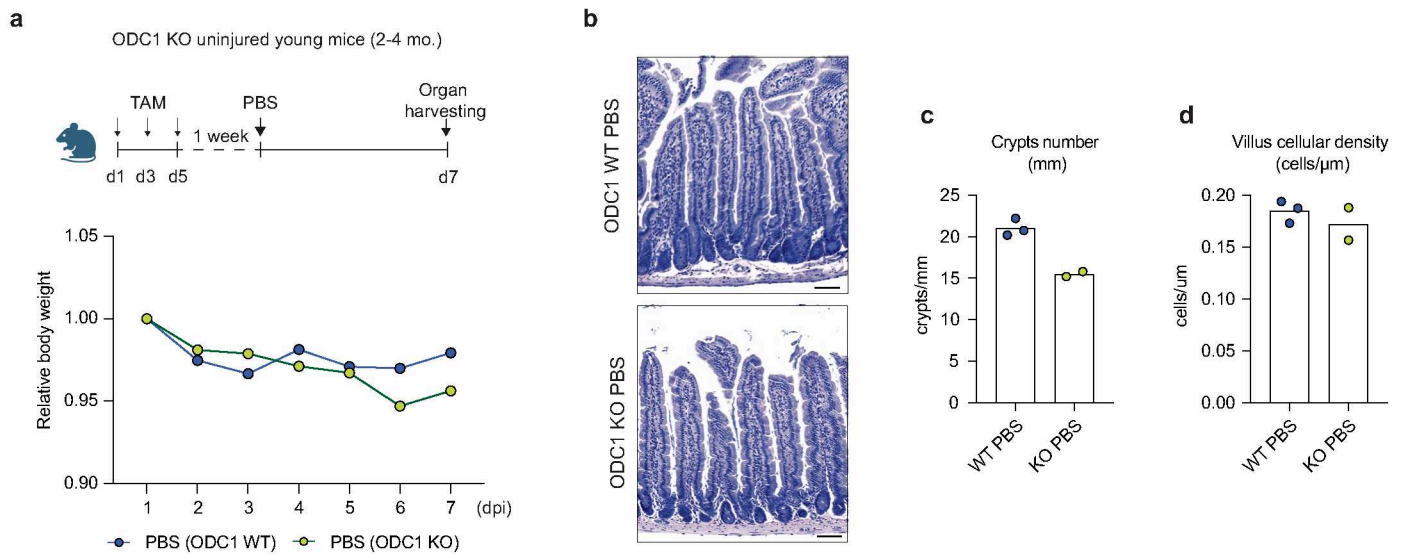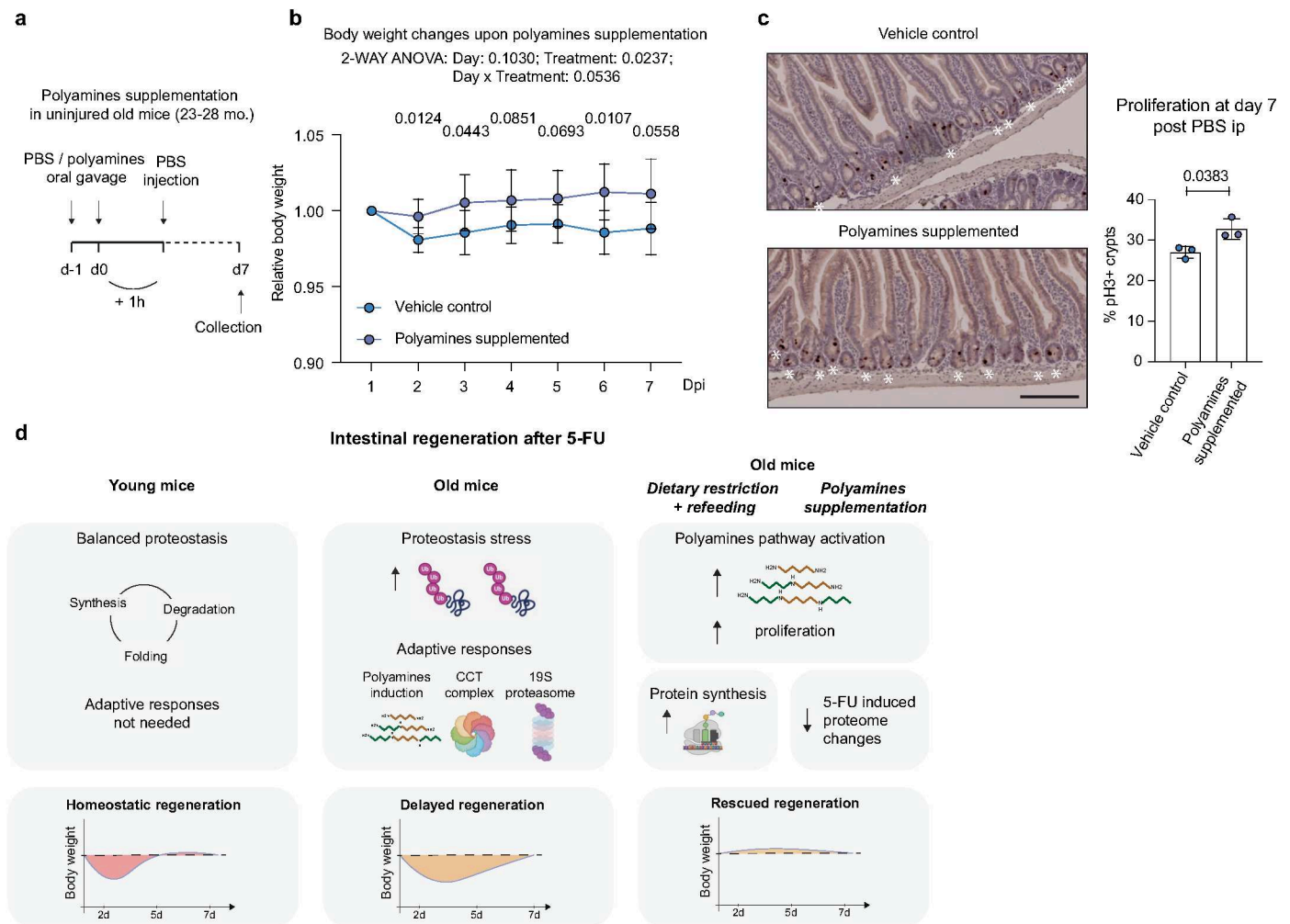
Extended Data Fig. 6 | Polyamines pathway deficiency in young, uninjured mice. a Upper: Schematic of ODC1 KO induction and PBS treatment (TAM: tamoxifen). Lower: Relative body weight of young ODC1 KO and WT mice treated with a single dose of PBS. Body weight of each mouse was normalized to its body weight at the day of injection. Data are presented as mean. n = 2 ODC1 KO, n = 3 ODC1 WT mice. **b** Representative HnE stainings of ODC1 KO and WT small intestines at 7 days post PBS injection. Scale bars, 50 μm. **c** Quantification of number of crypts per millimeter of small intestine in the indicated groups (7 dpi). Data are presented as mean. Each dot represents one mouse. n = 3 PBS ODC1 WT group; n = 2 PBS ODC1 KO group. **d** Quantification of number of cells per one micrometer of villi in the indicated groups (7 dpi). Data are presented as mean. Each dot represents one mouse. n = 3 PBS ODC1 WT group; n = 2 PBS ODC1 KO group. Panel **a** created with BioRender.com.
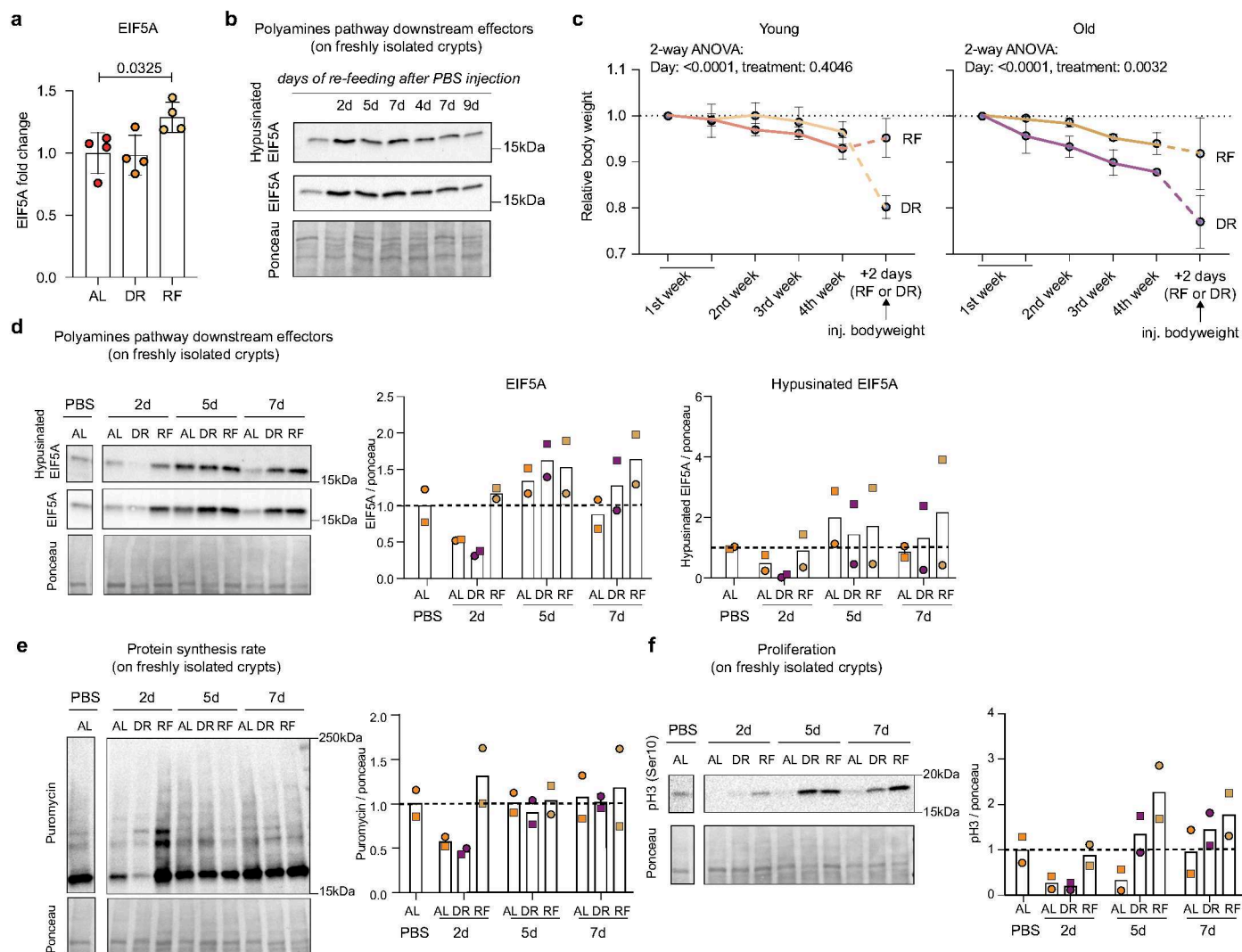
Extended Data Fig. 7 | Effect of dietary restriction followed by re-feeding on intestinal epithelium regeneration. a Quantification of EIF5A levels in intestinal crypts from old mice that underwent different dietary interventions. Based on proteomics data from Gebert et al. 2020[30]. Data are presented as mean ± SD. *p*-value was calculated by two-tailed Welch's t·test. *n* = 4 mice per group. **b** Immunoblot for hypusinated EIF5A and EIF5A proteins on freshly isolated crypts from old mice treated with PBS and re-feed at the indicated time points. **c** Relative body weight of young (left) and old (right) mice under DR for one month followed by two days of re-feeding or continuous DR prior to 5·FU or PBS injection. Body weight of each mouse was normalized to its body weight at the beginning of the dietary restriction period. *n* = 4 DR, *n* = 5 RF young mice and *n* = 4 DR, *n* = 3 RF old mice. Data are presented as mean ± SD. *p*-value was calculated using two-way ANOVA for overall day and treatment comparisons.

d Left: representative immunoblot for the hypusinated EIF5A and total EIF5A proteins on aged mice in the indicated groups. Right: Quantification of the hypusinated EIF5A and total EIF5A proteins relative to ponceau staining (loading control). Data are presented as mean. Each dot represents one mouse. *n* = 2 mice per group. **e** Left: Representative immunoblot for the puromycin incorporated proteins on aged mice in the indicated groups. Right: Quantification of the puromycin incorporation relative to ponceau staining (loading control). Data are presented as mean. Each dot represents one mouse. *n* = 2 mice per group. **f** Left: Representative immunoblot for the pH3 protein on aged mice in the indicated groups. Right: Quantification of pH3 protein relative to ponceau staining (loading control). Data are presented as mean. Each dot represents one mouse. *n* = 2 mice per group.

a

Polyamines supplementation
in uninjured old mice (23-28 mo.)

PBS / polyamines   PBS
oral gavage   injection

d-1 d0   d7

+ 1h

Collection

b

Body weight changes upon polyamines supplementation
2-WAY ANOVA: Day: 0.1030; Treatment: 0.0237;
Day x Treatment: 0.0536

0.0124
0.0443 0.0851   0.0107
0.0693   0.0558

Vehicle control
Polyamines supplemented

c

Vehicle control

Polyamines supplemented

Proliferation at day 7
post PBS ip

0.0383

d

Intestinal regeneration after 5-FU

Extended Data Fig. 8 | Effect of polyamines supplementation on uninjured intestinal epithelium. a Schematic of polyamines supplementation in uninjured old mice. Mice were orally gavaged with polyamines (polyamines supplemented) or PBS (vehicle control) before PBS injection. **b** Relative body weight of old mice orally gavaged with polyamines (polyamines supplemented) or PBS (vehicle control) before PBS injection. The body weight of each mouse was normalized to its body weight at the time of injection. $n = 6$ vehicle control group, $n = 8$ polyamines supplemented group. Data are presented as mean ± SD. p-value was calculated using two-tailed Welch's t-test for time point comparison and two-way ANOVA for overall comparisons. **c** Left: Representative pictures of immunohistochemistry (IHC) staining for pH3 at day 7 following polyamines supplementation. Scale bar, 200 μm. Asterisks indicate the pH3+ crypts.

Right: Change in % of pH3$^+$ crypt; $n = 3$ mice per group. Data are presented as mean ± SD. p-value was calculated using two-tailed Welch's t-test for group comparison. **d** Model of intestinal regeneration dynamics. Left: in young mice, injury leads to rapid small intestine regeneration and body weight recovery within ~5 days without proteostasis imbalance. Middle: in old mice, injury induces proteostasis stress, leading to delayed regeneration and body weight recovery (~day 7). Right: old mice subjected to 30 days of dietary restriction followed by 2 days of re-feeding, or directly supplemented with polyamines prior to injury, exhibit elevated polyamine levels and proliferation. This leads to improved protein synthesis, reduced proteomic alterations induced by 5-FU, and ultimately results in rescued body weight loss and improved intestinal regeneration. Panel **d** created with BioRender.com.

nature portfolio

Corresponding author(s):   Alessandro Ori, Francesco Neri

Last updated by author(s):   24.09.2025

Reporting Summary

Nature Portfolio wishes to improve the reproducibility of the work that we publish. This form provides structure for consistency and transparency in reporting. For further information on Nature Portfolio policies, see our Editorial Policies and the Editorial Policy Checklist.

Statistics

For all statistical analyses, confirm that the following items are present in the figure legend, table legend, main text, or Methods section.

n/a	Confirmed	
☐	☒	The exact sample size (*n*) for each experimental group/condition, given as a discrete number and unit of measurement
☐	☒	A statement on whether measurements were taken from distinct samples or whether the same sample was measured repeatedly
☐	☒	The statistical test(s) used AND whether they are one- or two-sided *Only common tests should be described solely by name; describe more complex techniques in the Methods section.*
☒	☐	A description of all covariates tested
☒	☐	A description of any assumptions or corrections, such as tests of normality and adjustment for multiple comparisons
☐	☒	A full description of the statistical parameters including central tendency (e.g. means) or other basic estimates (e.g. regression coefficient) AND variation (e.g. standard deviation) or associated estimates of uncertainty (e.g. confidence intervals)
☐	☒	For null hypothesis testing, the test statistic (e.g. *F*, *t*, *r*) with confidence intervals, effect sizes, degrees of freedom and *P* value noted *Give P values as exact values whenever suitable.*
☒	☐	For Bayesian analysis, information on the choice of priors and Markov chain Monte Carlo settings
☒	☐	For hierarchical and complex designs, identification of the appropriate level for tests and full reporting of outcomes
☐	☒	Estimates of effect sizes (e.g. Cohen's *d*, Pearson's *r*), indicating how they were calculated

Our web collection on statistics for biologists contains articles on many of the points above.

Software and code

Policy information about availability of computer code

Data collection	Axio Imager Zeiss, Molecular Imager ChemiDocTM XRS+Imaging system, CFX384 Touch Real-Time PCR System, Microsoft Excel for Mac; Xcalibur 4.3 and Tune version 2.0 (Thermo Fisher Scientific, Germany), FACS Aria II (BD Bioscience)
Data analysis	Image Lab 6.1 software, ZEN blue software v2, GraphPad Prism 10.0.3; R v4.1.3, RStudio Server v2024.04.0; Spectronaut v15.4, v16, v19 (Biognosys AG), FlowJo 10.7.1

For manuscripts utilizing custom algorithms or software that are central to the research but not yet described in published literature, software must be made available to editors and reviewers. We strongly encourage code deposition in a community repository (e.g. GitHub). See the Nature Portfolio guidelines for submitting code & software for further information.

Data

Policy information about availability of data

All manuscripts must include a data availability statement. This statement should provide the following information, where applicable:

- Accession codes, unique identifiers, or web links for publicly available datasets
- A description of any restrictions on data availability
- For clinical datasets or third party data, please ensure that the statement adheres to our policy

Source data is provided. MassIVE accession number for mass spectrometry based proteomics datasets is provided.
"Data availability

Research involving human participants, their data, or biological material

Policy information about studies with human participants or human data. See also policy information about sex, gender (identity/presentation), and sexual orientation and race, ethnicity and racism.

Reporting on sex and gender	N/A
Reporting on race, ethnicity, or other socially relevant groupings	N/A
Population characteristics	N/A
Recruitment	N/A
Ethics oversight	N/A N/A

Note that full information on the approval of the study protocol must also be provided in the manuscript.

Field-specific reporting

Please select the one below that is the best fit for your research. If you are not sure, read the appropriate sections before making your selection.

☒ Life sciences   ☐ Behavioural & social sciences   ☐ Ecological, evolutionary & environmental sciences

For a reference copy of the document with all sections, see nature.com/documents/nr-reporting-summary-flat.pdf

Life sciences study design

All studies must disclose on these points even when the disclosure is negative.

Sample size	No statistical methods were used to pre-determine sample size. Sample sizes were estimated based on preliminary experiments, with an effort to achieve a minimum of n=3 mice per treatment group which proved to be sufficient to reproducibly observe a statistical significant difference.
Data exclusions	No data was excluded.
Replication	All experiments were repeated in replicates and/or from different subjects in independent experiments. All attempts of replication were successful and yielded comparable outcomes.
Randomization	Mice were randomly assigned into treatment groups ensuring equal distribution among groups.
Blinding	The Investigators were not blinded to allocation during experiments and outcome assessment

Reporting for specific materials, systems and methods

We require information from authors about some types of materials, experimental systems and methods used in many studies. Here, indicate whether each material, system or method listed is relevant to your study. If you are not sure if a list item applies to your research, read the appropriate section before selecting a response.

Materials & experimental systems

n/a	Involved in the study
☐	☒ Antibodies
☒	☐ Eukaryotic cell lines
☒	☐ Palaeontology and archaeology
☐	☒ Animals and other organisms
☒	☐ Clinical data
☒	☐ Dual use research of concern
☒	☐ Plants

Methods

n/a	Involved in the study
☒	☐ ChIP-seq
☐	☒ Flow cytometry
☒	☐ MRI-based neuroimaging

Antibodies

Antibodies used	The following primary antibodies were used: Mouse-Puromycin (Millipore Sigma #MABE343), Rabbit-Ubiquitin linkage specific K48 (Abcam #ab140601), Rabbit-SQSTM1/p62 (Abcam #ab91526), Mouse-S6 ribosomal protein (Cell Signaling Technologies #2317), Mouse-Ubiquitin P4D1 (Santa Cruz Biotechnology #sc-8017), Rabbit-phospho Histone H3 (Cell Signaling Technologies #9701), Rabbit-phospho Histone H3 (Cell Signaling Technologies #3377), Rabbit-Hypusinated EIF5A (Millipore Sigma #ABS1064), Mouse-EIF5a (BD Biosciences #611977). Primary antibody dilutions for immunoblotting were done at 1:1000. The following secondary antibodies were used: Dako anti-rabbit #P0448 (dilution 1:2000), Dako anti-mouse #P0447 (dilution 1:1500), anti-rabbit IgG conjugated with AF594 (Thermo Fisher Scientific Cat#A-11012) (dilution 1:500)
Validation	All used antibodies were titrated. All the antibodies are validated for use in immunoblot or immunohistochemistry. Data are available at the manufacturer's website. All used antibodies are commercially available.

Animals and other research organisms

Policy information about studies involving animals; ARRIVE guidelines recommended for reporting animal research, and Sex and Gender in Research

Laboratory animals	Young (3–5 months old) and old (22–29 months old) male wild-type C57BL6/J mice obtained from Janvier or from internal breeding at the Leibniz Institute on Aging – Fritz Lipmann Institute (FLI) were used. Experiments were conducted according to protocols approved by the state government of Thuringia Thüringer Landesamt für Verbraucherschutz (TLV) authority (licenses number: FLI-20-003). Young (2-4 months) Odc1loxp/loxp; Villin-CreERT2 and Odc1wt/wt; Villin-CreERT2 mice were generated by crossing Odc1loxp/loxp mice to Villin-CreERT2 mice under the husbandry care of the Department of Comparative Medicine in Koch Institute for Integrative Cancer Research. Old (18 months old) male wild-type C57BL6/J mice were kept under the husbandry care of the Department of Comparative Medicine in Koch Institute for Integrative Cancer Research. Use of 5-FU, DFMO, CHX in Yilmaz lab was approved in the Committee on Animal Care (CAC) protocol at MIT.
Wild animals	This study did not involve wild animals.
Reporting on sex	Both male and female mice were used.
Field-collected samples	This study did not involve field-collected samples
Ethics oversight	Experiments on Young and Old C57BL6 mice were conducted according to protocols approved by the state government of Thuringia Thuringia Thüringer Landesamt für Verbraucherschutz (TLV) authority (licenses number: FLI-20-003). Injections of 5-FU, PBS on Odc1loxp/loxp; Villin-CreERT2 and Odc1wt/wt; Villin-CreERT2 mice and injections of 5-FU, PBS, CHX, DFMO on C57BL6/J mice were approved in the Committee on Animal Care (CAC) protocol at MIT.

Note that full information on the approval of the study protocol must also be provided in the manuscript.

Plants

Seed stocks	N/A
Novel plant genotypes	N/A
Authentication	N/A

Flow Cytometry

Plots

Confirm that:

☒ The axis labels state the marker and fluorochrome used (e.g. CD4-FITC).

☒ The axis scales are clearly visible. Include numbers along axes only for bottom left plot of group (a 'group' is an analysis of identical markers).

☒ All plots are contour plots with outliers or pseudocolor plots.

☒ A numerical value for number of cells or percentage (with statistics) is provided.

Methodology

Sample preparation	Intestinal organoids were dissociated to single cells by resuspending them in 1 ml of Single-Cell Isolation Solution (TrypLE supplemented with 1 mg/ml DNase I, 5 mM MgCl2, 80 μM Y27632) and incubated for 20 min at 37 °C with short vortexing after first 10 min of incubation. Reaction was quenched by addition of 29 ml ice-cold PBS and cells were centrifuged at 800 × g for 5 min at 4 °C. Cell pellet was resuspended in Facs staining media (PBS + fetal bovine serum 2% + EDTA 2.5 uM) supplemented with 80 μM Y27632. Single cells from intestinal organoids were then resuspended in 200μl of 1× binding buffer and 1μl of APC Annexin V from apoptosis detection Kit from BD Bioscience following incubation at RT for 15 min. After washing with 1× binding buffer, cells were resuspended in 1× binding buffer (100 μl) and analyzed using FACSAriaII (BD Biosciences). The sum of early and late apoptotic cells was used for quantification. All data were analyzed using FlowJo software.
Instrument	FACSAriaII (BD Biosciences)
Software	FlowJo 10.7.1. PRISM v.7.
Cell population abundance	Quantification of the sum of early and late apoptotic cells were reported in figure 3f
Gating strategy	The FACS gating strategy used for ANNEXIN V experiment in reported in supplementary figure X

☒ Tick this box to confirm that a figure exemplifying the gating strategy is provided in the Supplementary Information.